IEEE Access
Multidisciplinary ⋮ Rapid Review ⋮ Open Access Journal

Received February 15, 2022, accepted March 16, 2022, date of publication March 22, 2022, date of current version March 28, 2022.

Digital Object Identifier 10.1109/ACCESS.2022.3161543

Window Functions With Minimum-Sidelobe Derivatives for Computing Instantaneous Frequency

TSUBASA KUSANO, (Graduate Student Member, IEEE), KOHEI YATABE, (Member, IEEE), AND YASUHIRO OIKAWA, (Member, IEEE)
Department of Intermedia Art and Science, Waseda University, Tokyo 169-8555, Japan

Corresponding author: Tsubasa Kusano (tsubasa.k@suou.waseda.jp)

This work was supported by the Japan Society for the Promotion of Science (JSPS) KAKENHI under Grant 19J21839.

ABSTRACT In the field of nonstationary signal analysis and processing, the short-time Fourier transform (STFT) is frequently used to convert signals into the time-frequency domain. The instantaneous frequency (IF) of the STFT is defined as the time derivative of the STFT phase and plays an important role in the reassignment method and the synchrosqueezing transform (SST). In this paper, we propose a framework to design a window function for computing the IF of STFT. Computing the IF requires the STFT with a window and STFT with its derivative, i.e., the IF computation depends on both the window function and its derivative. To design a window suitable for computing the IF, we formulate the window design problem as a sidelobe minimization problem of the corresponding derivative. Two windows are designed considering the sidelobe energy or the highest sidelobe level as cost functions for minimizing the sidelobes of their derivatives. The SST using the proposed window provides a sharper time-frequency representation compared to those produced using ordinary bandwidth-adjustable windows.

INDEX TERMS Short-time Fourier transform (STFT), instantaneous frequency (IF), window derivative, adjustable window, synchrosqueezing transform (SST).

I. INTRODUCTION

Time-frequency (T-F) representations are highly important in nonstationary signal analysis and processing. The short-time Fourier transform (STFT) is widely used to convert a signal into the T-F domain, owing to its simplicity and well-understood structure [1]–[4]. The resolution of a T-F representation obtained by the STFT is limited by Heisenberg's uncertainty principle. To adjust its resolution, many window functions have been proposed from various viewpoints, such as frequency responses [5]–[14] and numerical stability in signal processing [15]–[20].

The reassignment method and the synchrosqueezing transform (SST) have been proposed to overcome Heisenberg's uncertainty principle [21]. The reassignment method was first proposed by Kodera to improve the readability of the T-F representation obtained by the STFT [22]. Then, Auger and Flandrin popularized the reassignment method by discovering an efficient computational method; furthermore, they generalized the reassignment method to T-F representations in Cohen's class and time-scale representations [23]. Then, the reassignment method was generalized for any filterbank [24], [25]. The reassignment method sharpens a T-F representation using the time and frequency derivatives of its phase at the expense of invertibility. The time and frequency derivatives of the STFT phase are referred to as the instantaneous frequency (IF) and group delay, respectively.

In the context of audio signal analysis, Daubechies and Maes proposed the SST [26], [27], which is a variant of the reassignment method. The SST performs frequency-only reassignment to a complex-valued T-F representation to sharpen the T-F representation while ensuring invertibility. Subsequently, the SST was also generalized for STFT [28], [29] and other representations [25], [30] and has been widely studied [31]–[35]. The FSST reassigns the spread components using the IF, which is affected by the window function. Therefore, to improve the performance of the FSST, the

The associate editor coordinating the review of this manuscript and approving it for publication was Lin Wang.

window should be designed considering the computation of the IF.

Moreover, IF has also been employed in other applications, such as a phase vocoder [36]–[39], T-F mask estimation [40], [41], phase conversion [42]–[45], and speech processing [46]–[48]. In the context of a phase vocoder, the effect of a window on the IF computation has been demonstrated by comparing several existing windows [38]. Therefore, designing a window for computing the IF can also improve the performance of its applications.

A method to compute the IF uses the STFTs with a window and with its (time-)derivative [23], which can compute accurately even in a discrete setting. That is, the computed IF depends on both the window and its derivative. Furthermore, interference of multiple signal components influences the IF computation. To reduce the interference of multiple signal components, the window and its derivative should be designed to reduce the T-F spreading under Heisenberg's uncertainty.

The main purpose of a window design for reducing spreading is its frequency response because the spread in the time direction can be controlled relatively easily by the support of the window. Hence, the sidelobes of the frequency responses of the window and its derivative need to be reduced. In particular, the sidelobes of the window derivative should be given more attention since the differential operator emphasizes high-frequency components. Several window functions are designed by considering the continuity at their edges, which is related to the sidelobe of their derivatives [13], [14]. However, no method has explicitly considered the frequency response of the window derivative. Designing a window function to minimize the sidelobes of the frequency response of its derivative is expected to obtain a window function that is more suitable for IF computation.

Therefore, in this paper, we propose a framework for designing a window function for IF computation. The proposed method first designs the window derivative to minimize the sidelobes and then estimates the window function from the designed window derivative. The designed windows are evaluated by the IF computation and an application to the FSST.

This paper aims to expand on our five-page conference paper [49], in which we proposed a window function that is designed to minimize the sidelobe energy of its derivative and validated its performance in limited experiments. The contribution of this paper is summarized as follows:

- A detailed explanation about computing IF in continuous and discrete STFT (Sec. II).
- An additional proposed window is designed to minimize the highest sidelobe level of its derivative (Sec. IV-C).
- A proposed window estimation method from the window derivative for minimizing the truncation effect (Sec. IV-D).
- Detailed evaluations of the proposed windows in terms of computing IF (Sec. VI).

TABLE 1. List of notations.

Symbol	Description
$\mathbb{R}$	Set of all real numbers
$\mathbb{C}$	Set of all complex numbers
$L^2(\mathbb{R})$	Space of square integrable functions
$C^\rho(\mathbb{R})$	Set of all ρ times continuously differentiable functions
$f(x)$	Value of a function f at x
$\mathbf{x}[n]$	nth element of a vector $\mathbf{x}$
$\mathbf{X}[n,m]$	(n,m)th element of a matrix $\mathbf{X}$
$\overline{(\cdot)}$	Complex conjugate
$(\cdot)^{\mathrm{T}}$	Transpose
$(\cdot)^*$	Conjugate transpose
$\langle \mathbf{x}, \mathbf{y} \rangle$	Inner product of $\mathbf{x}, \mathbf{y} \in \mathbb{C}^L$; $\langle \mathbf{x}, \mathbf{y} \rangle = \mathbf{y}^* \mathbf{x}$
$\|\cdot\|$	Euclidean norm
$\mathbf{1}_N$	N-dimensional vector whose elements are all one
$\mathbf{I}_N$	$N \times N$ identity matrix
$\mathbf{O}_{N,M}$	$N \times M$ zero matrix
$\Re\{z\}$	Real part of z
$\Im\{z\}$	Imaginary part of z
$\mathrm{Arg}\{z\}$	(Principal value of) complex argument of z
$\mathrm{diag}(\mathbf{x})$	Diagonal matrix whose diagonal elements are $\mathbf{x}$
$\lfloor x \rceil$	Round function that rounds x to the nearest integer
$\lfloor x \rfloor$	Floor function
$\mathrm{sign}(x)$	Sign function; $\mathrm{sign}(x) = \begin{cases} \frac{x}{\lvert x \rvert} & \text{if } x \neq 0 \\ 0 & \text{if } x = 0 \end{cases}$

TABLE 2. List of abbreviations.

Abbreviation	Meaning
T-F	Time-frequency
STFT	Short-time Fourier transform
SST	Synchrosqueezing transform
FSST	Fourier synchrosqueezing transform
IF	Instantaneous frequency
DFT	Discrete Fourier transform
SE	Sidelobe energy
HSL	Highest sidelobe level

- Quantitative evaluations of FSST using the Rényi entropy and the Earth mover's distance (Sec. VII).

The rest of this paper is organized as follows. Sections II and III introduce the IF of the STFT and bandwidth-adjustable windows, respectively. Then, Section IV explains our proposed method for designing windows. Section V presents the frequency responses of windows designed by the proposed method. Section VI provides numerical experiments to evaluate the performance of the designed windows in terms of computing the IF. Section VII presents the performance of applying the designed window to the FSST, and the conclusion of this paper is presented in Section VIII.

II. PRELIMINARY

A. NOTATION

The list of notations and abbreviations used in this paper are summarized in Tables 1 and 2, respectively. We define the frequency response of a discrete signal $\mathbf{f} \in \mathbb{C}^L$ as

$$(\mathcal{F}\mathbf{f})(\omega) := \sum_{l=0}^{L-1} \mathbf{f}[l] \mathrm{e}^{-\mathrm{i}2\pi\omega l}, \tag{1}$$

where i is the imaginary unit. The discrete Fourier transform (DFT) $\mathbf{F} : \mathbb{C}^L \to \mathbb{C}^L$ is defined as

$$\hat{\mathbf{f}}[m] := (\mathbf{F}\mathbf{f})[m] = \sum_{l=0}^{L-1} \mathbf{f}[l] \mathrm{e}^{-\mathrm{i}\frac{2\pi ml}{L}}, \tag{2}$$

and its inverse $\mathbf{F}^{-1} : \mathbb{C}^L \to \mathbb{C}^L$ is given by

$$\mathbf{f}[l] = (\mathbf{F}^{-1}\hat{\mathbf{f}})[l] = \frac{1}{L} \sum_{m=0}^{L-1} \hat{\mathbf{f}}[m] \mathrm{e}^{\mathrm{i}\frac{2\pi ml}{L}}. \tag{3}$$

B. COMPUTING IF USING STFT

The STFT of a signal $f \in L^2(\mathbb{R})$ with a window function $g \in L^2(\mathbb{R}) \cap C^1(\mathbb{R})$ is defined as

$$(\mathcal{V}_g f)(t, \omega) := \int_{\mathbb{R}} f(\tau) \overline{g(\tau - t)} \mathrm{e}^{-\mathrm{i}2\pi\omega\tau} \mathrm{d}\tau, \tag{4}$$

where $t \in \mathbb{R}$ and $\omega \in \mathbb{R}$ represent time and frequency, respectively. The STFT can be represented as

$$(\mathcal{V}_g f)(t, \omega) = \mathcal{M}_g^f(t, \omega) \cdot \mathrm{e}^{\mathrm{i}2\pi \Phi_g^f(t,\omega)}, \tag{5}$$

where $\mathcal{M}_g^f := |\mathcal{V}_g f|$ is the STFT magnitude, and Φ_g^f is the STFT phase. The IF of the STFT is defined as the time derivative of the phase [50], [51],

$$\mathrm{IF}_g^f(t, \omega) := \frac{\partial}{\partial t} \Phi_g^f(t, \omega). \tag{6}$$

For instance, let us consider the IF of a continuous sinusoid

$$s(t) = A_{\mathbf{s}} \mathrm{e}^{\mathrm{i}(2\pi\xi_{\mathbf{s}} t + \phi_{\mathbf{s}})}. \tag{7}$$

The STFT of $s(t)$ is explicitly expressed as

$$\begin{aligned}(\mathcal{V}_g s)(t, \omega) &= A_{\mathbf{s}} \mathrm{e}^{\mathrm{i}\phi_{\mathbf{s}}} \int_{\mathbb{R}} \overline{g(\tau - t)} \mathrm{e}^{-\mathrm{i}2\pi(\omega - \xi_{\mathbf{s}})\tau} \mathrm{d}\tau \\ &= A_{\mathbf{s}} \mathrm{e}^{\mathrm{i}\phi_{\mathbf{s}} - \mathrm{i}2\pi(\omega - \xi_{\mathbf{s}})t} \int_{\mathbb{R}} \overline{g(\tau)} \mathrm{e}^{-\mathrm{i}2\pi(\omega - \xi_{\mathbf{s}})\tau} \mathrm{d}\tau \\ &= \overline{\hat{g}(\xi_{\mathbf{s}} - \omega)} A_{\mathbf{s}} \mathrm{e}^{\mathrm{i}\phi_{\mathbf{s}} - \mathrm{i}2\pi(\omega - \xi_{\mathbf{s}})t}, \end{aligned} \tag{8}$$

where $\hat{g}(\omega)$ is the Fourier transform of $g(t)$. Then, its phase is given by

$$\Phi_g^s(t, \omega) = \frac{\phi_{\mathbf{s}} + \mathrm{Arg}\left\{\overline{\hat{g}(\xi_s - \omega)}\right\}}{2\pi} - (\omega - \xi_{\mathbf{s}})t. \tag{9}$$

Consequently, the IF of $s(t)$ is calculated as

$$\mathrm{IF}_g^s(t, \omega) = \frac{\partial}{\partial t} \Phi_g^s(t, \omega) = \xi_{\mathbf{s}} - \omega. \tag{10}$$

This corresponds to the difference between the frequency of the sinusoid $\xi_{\mathbf{s}}$ and the frequency axis ω, which allows us to observe detailed frequency information from the spread T-F representation obtained by the STFT. Some studies refer to it as *the relative instantaneous frequency* [52].[1]

The straightforward approach for computing IF_g^f from (6) in the discrete setting is an approximation of the time derivative of the phase by finite differences. However, this suffers from the phase unwrapping problem [53]. Avoiding such problems, [23] proposed an alternative expression of the IF given by

$$\mathrm{IF}_g^f = \frac{1}{2\pi} \Im \left\{ \frac{1}{\mathcal{V}_g f} \cdot \frac{\partial}{\partial t} \mathcal{V}_g f \right\} = -\frac{1}{2\pi} \Im \left\{ \frac{\mathcal{V}_{g'} f}{\mathcal{V}_g f} \right\}, \tag{11}$$

where $g' = \mathrm{d}g/\mathrm{d}t$ is the derivative of the window g. This is derived from the following calculation using the chain rule:

$$\begin{aligned}\frac{\partial}{\partial t}(\mathcal{V}_g f)(t, \omega) &= \mathrm{e}^{\mathrm{i}2\pi\Phi_g^f} \cdot \frac{\partial}{\partial t} \mathcal{M}_g^f + \mathcal{M}_g^f \mathrm{e}^{\mathrm{i}2\pi\Phi_g^f} \cdot \mathrm{i}2\pi \frac{\partial}{\partial t} \Phi_g^f \\ &= \mathrm{e}^{\mathrm{i}2\pi\Phi_g^f} \cdot \frac{\partial}{\partial t} \mathcal{M}_g^f + \mathcal{V}_g f \cdot \mathrm{i}2\pi \frac{\partial}{\partial t} \Phi_g^f. \end{aligned} \tag{12}$$

In addition, the derivative of the STFT with respect to time can be rewritten as

$$\begin{aligned}\frac{\partial}{\partial t}(\mathcal{V}_g f)(t, \omega) &= -\int_{\mathbb{R}} f(\tau) \overline{\frac{\mathrm{d}g}{\mathrm{d}t}(\tau - t)} \mathrm{e}^{-\mathrm{i}2\pi\omega\tau} \mathrm{d}\tau \\ &= -(\mathcal{V}_{g'} f)(t, \omega). \end{aligned} \tag{13}$$

According to (11), computing the IF requires the STFT using the window function g and its derivative g'. Hence, the computed IF depends on both windows.

C. COMPUTING IF IN DISCRETE STFT

The discrete version of the STFT for a discrete signal $\mathbf{f} \in \mathbb{C}^L$ with a discrete window function $\mathbf{g} \in \mathbb{C}^L$ is written as

$$(\mathbf{V}_{\mathbf{g}}\mathbf{f})[n, m] := \sum_{l=0}^{L-1} \mathbf{f}[l] \overline{\mathbf{g}[l - n]} \mathrm{e}^{-\mathrm{i}\frac{2\pi ml}{L}} \tag{14}$$

where $n = 0, 1, \ldots, L-1$ is the time-shift index and $m = 0, 1, \ldots, L-1$ is the modulation index. $\mathbf{g}[l]$ outside the domain $[0, L-1]$ is evaluated as an L-periodic sequence [2], i.e.,

$$\mathbf{g}[l + L] = \mathbf{g}[l]. \tag{15}$$

As in (11), the IF of the discrete STFT can be computed by the window $\mathbf{g}$ and its spectral derivative $\mathbf{g}' = \mathbf{D}\mathbf{g}$,

$$\mathrm{IF}_{\mathbf{g}}^{\mathbf{f}}[n, m] = -\frac{1}{2\pi} \Im \left\{ \frac{(\mathbf{V}_{\mathbf{g}'}\mathbf{f})[n, m]}{(\mathbf{V}_{\mathbf{g}}\mathbf{f})[n, m]} \right\}. \tag{16}$$

The spectral differentiation operator $\mathbf{D}$ is defined as

$$\begin{aligned}(\mathbf{D}\mathbf{g})[l] &:= \frac{1}{L} \sum_{m=0}^{L-1} \mathbf{d}[m] \hat{\mathbf{g}}[m] \mathrm{e}^{\mathrm{i}\frac{2\pi lm}{L}} \\ &= (\mathbf{F}^{-1} \,\mathrm{diag}(\mathbf{d})\mathbf{F}\mathbf{g})[l], \end{aligned} \tag{17}$$

where

$$\mathbf{d}[m] := \begin{cases} \mathrm{i}2\pi m/L, & \text{if } 0 \le m < L/2 \\ 0, & \text{if } m = L/2 \\ \mathrm{i}2\pi(m - L)/L, & \text{if } L/2 < m \le L - 1 \end{cases} \tag{18}$$

The rationale for using the spectral derivative as a counterpart to the continuous-time derivative is given by [24].[2]

[1] This comes from defining STFT as (4), and other definitions will change this expression. More details are given in [45].

[2] To be precise, [24] considered a counterpart of the continuous-time derivative for an infinite-length sequence. The rationale for using the spectral derivative was derived by a straightforward adaptation of [24] for a discrete and finite-length signal.

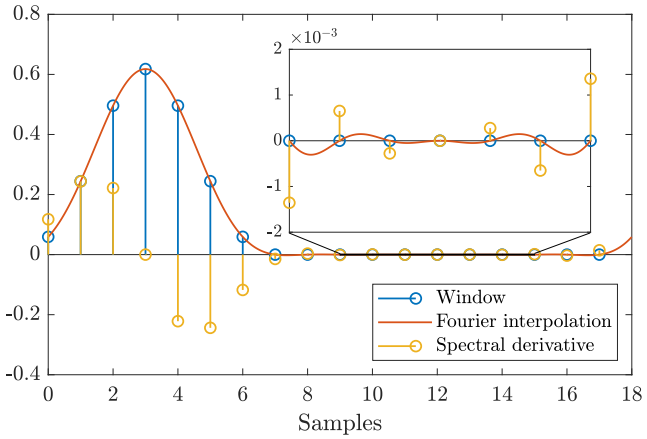

FIGURE 1. Spectral differentiation of a window function supported on $[0, N-1]$ $(N = 7)$.

An example of a window function and its derivative obtained by spectral differentiation is illustrated in Fig. 1. In Fig. 1, the signal length is $L = 18$, and the window is supported on $[0, N-1]$ $(N = 7)$. The spectral differentiation corresponds to the differentiation of a function obtained by the Fourier interpolation of a discrete signal. A function obtained by the Fourier interpolation of the window oscillates slightly outside of $[0, N-1]$, even if the window is supported on $[0, N-1]$. Therefore, the support of the window does not coincide with the support of its derivative. In general, the spectral derivative of a window supported on $[0, N-1]$ does not have the same support when $N < L$. When $N = L$, the STFT requires computing the DFT of the entire signal, which reduces its applicability to real-time processing or lengthy signal analysis [54]–[56]. In practice, the window derivative is truncated to have the same support as the original window.

D. COMPARISON OF SPECTRAL AND ANALYTICAL DERIVATIVES

When the window function is initially defined as a differentiable continuous function, an alternative to spectral differentiation is to calculate the window derivative analytically and sample the derivative. Let us illustrate this method using the Hann window, which is one of the most famous of such window functions. The Hann window supported on $[0, N-1]$ is defined as

$$g(t) = \begin{cases} \frac{1}{2}\left(1 - \cos\left(\frac{2\pi t}{N-1}\right)\right), & \text{if } t \in [0, N-1] \\ 0, & \text{otherwise.} \end{cases} \tag{19}$$

Its analytical derivative is given by

$$g'(t) = \begin{cases} \frac{\pi}{N-1}\sin\left(\frac{2\pi t}{N-1}\right), & \text{if } t \in [0, N-1] \\ 0, & \text{otherwise.} \end{cases} \tag{20}$$

Here, we compare the spectral and analytical derivatives in terms of the computed IF of a sinusoid. Considering a discrete complex sinusoid

$$\mathbf{s}[l] = A_{\mathbf{s}} \mathrm{e}^{\mathrm{i}(2\pi\xi_{\mathbf{s}} l + \phi_{\mathbf{s}})}, \tag{21}$$

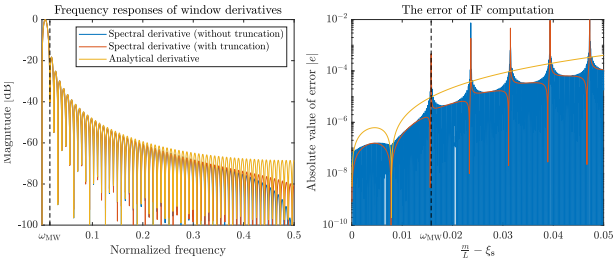

FIGURE 2. Comparison of derivatives of the Hann window. The left and right sides show the frequency responses of the window derivatives and the errors of the IF computation using these window derivatives.

for $l = 0, 1, \ldots, L-1$, we evaluated the error between the analytical IF of the sinusoid (10) and the computed IF

$$e[n, m] = \left(\xi_{\mathbf{s}} - \frac{m}{L}\right) - \mathrm{IF}^{\mathbf{s}}_{\mathbf{g}}[n, m]. \tag{22}$$

With the same manipulations in (8), the STFT of sinusoid $\mathbf{s}$ is calculated as

$$(\mathbf{V}_{\mathbf{g}}\mathbf{s})[n, m] = \overline{(\mathcal{F}\mathbf{g})\left(\xi_{\mathbf{s}} - \frac{m}{L}\right)} A_{\mathbf{s}} \mathrm{e}^{\mathrm{i}\phi_{\mathbf{s}} - \mathrm{i}2\pi\left(\frac{m}{L} - \xi_{\mathbf{s}}\right)n}. \tag{23}$$

Then, the IF of sinusoid $\mathbf{s}$ is calculated as

$$\begin{aligned} \mathrm{IF}^{\mathbf{s}}_{\mathbf{g}}[n, m] &= -\frac{1}{2\pi}\Im\left\{\frac{(\mathbf{V}_{\mathbf{g}'}\mathbf{s})[n, m]}{(\mathbf{V}_{\mathbf{g}}\mathbf{s})[n, m]}\right\} \\ &= -\frac{1}{2\pi}\Im\left\{\frac{\overline{(\mathcal{F}\mathbf{g}')(\xi_{\mathbf{s}} - \frac{m}{L})}}{\overline{(\mathcal{F}\mathbf{g})(\xi_{\mathbf{s}} - \frac{m}{L})}}\right\}, \end{aligned} \tag{24}$$

which is independent of the time index n. When $\mathbf{g}$ is real-valued, (24) is simplified as

$$\mathrm{IF}^{\mathbf{s}}_{\mathbf{g}}[n, m] = -\frac{1}{2\pi}\Im\left\{\frac{(\mathcal{F}\mathbf{g}')(\frac{m}{L} - \xi_{\mathbf{s}})}{(\mathcal{F}\mathbf{g})(\frac{m}{L} - \xi_{\mathbf{s}})}\right\}. \tag{25}$$

Thus, the error (22) is rewritten as

$$e[m] = \left(\xi_{\mathbf{s}} - \frac{m}{L}\right) + \frac{1}{2\pi}\Im\left\{\frac{(\mathcal{F}\mathbf{g}')(\frac{m}{L} - \xi_{\mathbf{s}})}{(\mathcal{F}\mathbf{g})(\frac{m}{L} - \xi_{\mathbf{s}})}\right\}. \tag{26}$$

Fig. 2 shows the frequency responses of the window derivatives and errors of IF computation using these window derivatives. The window length and the signal length were set to $N = 2^7$ and $L = 2^{12}$. The mainlobe width ω_{MW} is defined as the first null point of the frequency response except for $\omega = 0$. The error in the IF computed by the analytical derivative is larger than that of the spectral derivative. Therefore, this paper focuses on spectral differentiation, even if these windows are analytically differentiable.

III. BANDWIDTH-ADJUSTABLE WINDOWS

One aim of the window design is to control T-F spreading under Heisenberg's uncertainty principle. The spread in the time direction can be controlled by setting the length of the window function. We assume that a window $\mathbf{g}$ is supported on $[0, N-1]$ and let $\mathbf{w} \in \mathbb{C}^N$ denote its nonzero part, i.e.,

$$\mathbf{g}[l] = \begin{cases} \mathbf{w}[l], & \text{if } l = 0, 1, \ldots, N-1 \\ 0, & \text{otherwise.} \end{cases} \tag{27}$$

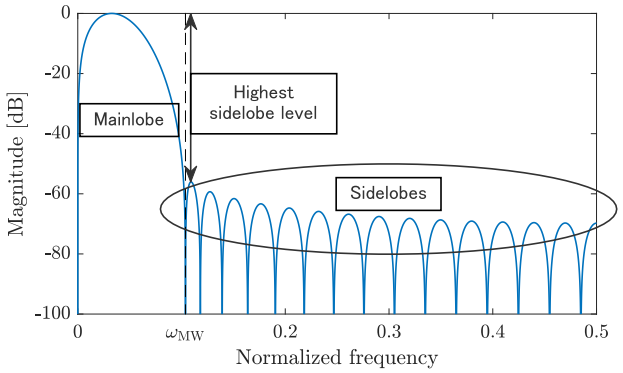

FIGURE 3. Sidelobe energy and highest sidelobe level of a window function.

To obtain a well-localized T-F representation, a window should be designed so that its frequency response has a narrow mainlobe and low sidelobe levels under the defined window length N. However, a window function has a trade-off between the mainlobe width and the sidelobe level. The mainlobe width is closely related to the appearance of the T-F representation and can be intuitively chosen according to the application. Thus, the sidelobe characteristics should be optimized under the mainlobe width ω_{MW} chosen according to the application. The sidelobe energy (SE) and highest sidelobe level (HSL) are used to evaluate the localization of the frequency response of the window functions, which are defined as

$$\mathrm{SE} = 10\log_{10}\frac{\int_{-\frac{1}{2}}^{\frac{1}{2}} \mathcal{W}_{\omega_{\mathrm{MW}}}(\omega)\,|(\mathcal{F}\mathbf{w})(\omega)|^2\,\mathrm{d}\omega}{\int_{-\frac{1}{2}}^{\frac{1}{2}} |(\mathcal{F}\mathbf{w})(\omega)|^2\,\mathrm{d}\omega}, \tag{28}$$

$$\mathrm{HSL} = 10\log_{10}\frac{\max_{\omega}\,\mathcal{W}_{\omega_{\mathrm{MW}}}(\omega)\,|(\mathcal{F}\mathbf{w})(\omega)|^2}{\max_{\omega}\,|(\mathcal{F}\mathbf{w})(\omega)|^2}, \tag{29}$$

where $\mathcal{W}_{\omega_{\mathrm{MW}}}(\omega)$ is a weight function,

$$\mathcal{W}_{\omega_{\mathrm{MW}}}(\omega) = \begin{cases} 0, & \text{if } |\omega| < \omega_{\mathrm{MW}} \\ 1, & \text{if } |\omega| \geq \omega_{\mathrm{MW}}. \end{cases} \tag{30}$$

The SE and HSL of a window function are shown in Fig. 3.

Many windows, such as the rectangular window, Bartlett window, Hann window, Blackman window, and Nuttall window [13] depend only on the window length. However, some window functions contain additional parameters for adjusting the bandwidth; these are referred to as *adjustable windows*. The Dolph–Chebyshev window [5], the Slepian window [6], the Kaiser window [8], the Saramäki window [9], the ultraspherical window [10], [11], the cosh window [12], and the Tukey window (tapered cosine window) [57] belong to this class. Among them, the Slepian window and the Dolph–Chebyshev window are characterized by the following optimization problems:

$$\underset{\mathbf{w}}{\text{minimize}} \quad \frac{\int_{-\frac{1}{2}}^{\frac{1}{2}} \mathcal{W}_W(\omega)\,|(\mathcal{F}\mathbf{w})(\omega)|^2\,\mathrm{d}\omega}{\int_{-\frac{1}{2}}^{\frac{1}{2}} |(\mathcal{F}\mathbf{w})(\omega)|^2\mathrm{d}\omega}, \tag{31}$$

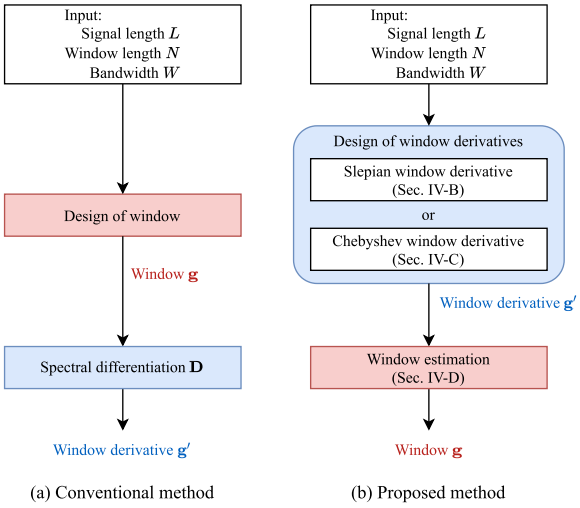

FIGURE 4. Block diagrams of (a) the conventional computation of a window function and a window derivative pair and (b) the proposed method.

$$\underset{\mathbf{w}}{\text{minimize}} \quad \frac{\max_{\omega\in[-\frac{1}{2},\frac{1}{2}]}\ \mathcal{W}_W(\omega)|(\mathcal{F}\mathbf{w})(\omega)|}{\max_{\omega\in[-\frac{1}{2},\frac{1}{2}]}\ |(\mathcal{F}\mathbf{w})(\omega)|}, \tag{32}$$

respectively, where $W \in (0, \frac{1}{2}]$. These windows are designed to have a well-localized frequency response in terms of SE and HSL, and they certainly show better characteristics than other window functions (as indicated in the left side of Fig. 10).

IV. PROPOSED METHOD

We now propose a window design method to reduce the influence of the sidelobes of the window derivative on the IF computation. A comparison between the conventional and proposed methods of computing a window function and a window derivative pair is illustrated in Fig. 4. In general, to obtain a window and its derivative, the window function is first designed, and then the window derivative is calculated by differentiating the designed window [Fig. 4 (a)]. By contrast, our method first designs the window derivative to minimize the sidelobes and then estimates the window function from the window derivative [Fig. 4 (b)].

A. PROBLEM FORMULATION

To restrict the spread in the time direction, we assume that the window derivative is supported on $[0, N-1]$, i.e.,

$$\mathbf{g}'[l] = \begin{cases} \mathbf{z}[l], & \text{if } l = 0, 1, \ldots, N-1 \\ 0, & \text{otherwise}, \end{cases} \tag{33}$$

where $\mathbf{z} \in \mathbb{C}^N$ corresponds to the nonzero part of $\mathbf{g}'$. Calculating the window derivative from the window function can be performed straightforwardly by spectral differentiation. Conversely, from $\mathbf{z}$ such that $\langle \mathbf{z}, \mathbf{1}_N \rangle = 0$, $\mathbf{g}$ can be calculated as the spectral integration:

$$\mathbf{g} = \mathbf{F}^{-1}\,\mathrm{diag}(\mathbf{b})\mathbf{F}\mathbf{P}_{L,N}\mathbf{z} + c\mathbf{1}_L, \tag{34}$$

where

$$\mathbf{b}[m] := \begin{cases} 0, & m = 0 \\ -\mathrm{i}L/2\pi m, & \text{if } 0 < m < L/2 \\ 0, & \text{if } m = L/2 \\ -\mathrm{i}L/2\pi(m-L), & \text{if } L/2 < m \leq L-1, \end{cases}$$

$\mathbf{P}_{L,N} \in \mathbb{R}^{L\times N}$ is the zero-padding matrix,

$$\mathbf{P}_{L,N} := \left[\mathbf{I}_N, \mathbf{O}_{N,L-N}\right]^{\mathrm{T}}, \tag{35}$$

and c is an integral constant. $\langle \mathbf{z}, \mathbf{1}_N \rangle = 0$ constrains the integration of the Fourier series to also be a Fourier series. Therefore, we formulate the design of the window derivative as

$$\begin{aligned} &\underset{\mathbf{z}}{\text{minimize}} \ \ \Theta(\mathbf{z}) \\ &\text{subject to } \langle \mathbf{z}, \mathbf{1}_N \rangle = 0, \end{aligned} \tag{36}$$

where $\Theta(\mathbf{z})$ is an objective function measuring the sidelobes of the frequency response of $\mathbf{z}$, which corresponds to the SE or HSL of $\mathbf{z}$. In summary, we first design the window derivative $\mathbf{z}$ by (36) and then estimate the window function from $\mathbf{z}$ by (34).

In the remainder of this section, Sec. IV-B and Sec. IV-C, we explain the methods for designing the window derivative to minimize the SE and HSL, respectively. Estimating the original window $\mathbf{w}$ from the designed window derivative $\mathbf{z}$ is introduced in Sec. IV-D. Hereafter, the window derivatives minimizing the SE and HSL are referred to as the *Slepian window derivative* and the *Chebyshev window derivative*, respectively.

B. SLEPIAN WINDOW DERIVATIVE

This subsection explains the design of the Slepian window derivative. Considering the case where the cost function $\Theta(\mathbf{z})$ in (36) is the ratio of the energy outside $[-W, W]$ to the total energy, the design problem of the Slepian window derivative is formulated as

$$\begin{aligned} &\underset{\mathbf{z}}{\text{minimize}} \ \ \frac{\int_{-\frac{1}{2}}^{\frac{1}{2}} \mathcal{W}_W(\omega)\, |(\mathcal{F}\mathbf{z})(\omega)|^2 \, \mathrm{d}\omega}{\int_{-\frac{1}{2}}^{\frac{1}{2}} |(\mathcal{F}\mathbf{z})(\omega)|^2 \mathrm{d}\omega} \\ &\text{subject to } \langle \mathbf{z}, \mathbf{1}_N \rangle = 0. \end{aligned} \tag{37}$$

The cost function in Eq. (37) can be rewritten as the Rayleigh quotient:

$$\frac{\mathbf{z}^{\mathrm{T}}\mathbf{z} - \mathbf{z}^{\mathrm{T}}\mathbf{S}_N\mathbf{z}}{\mathbf{z}^{\mathrm{T}}\mathbf{z}} = 1 - \frac{\mathbf{z}^{\mathrm{T}}\mathbf{S}_N\mathbf{z}}{\mathbf{z}^{\mathrm{T}}\mathbf{z}}, \tag{38}$$

where $\mathbf{S}_N \in \mathbb{R}^{N\times N}$ is a real-symmetric matrix whose elements are given by

$$\mathbf{S}_N[m,n] = 2W\,\mathrm{sinc}(2W(m-n)), \tag{39}$$

$$\mathrm{sinc}(x) := \begin{cases} \dfrac{\sin(\pi x)}{\pi x}, & \text{if } x \neq 0 \\ 1, & \text{if } x = 0. \end{cases} \tag{40}$$

Fixing $\mathbf{z}^{\mathrm{T}}\mathbf{z} = 1$ and reducing the constant 1 not relevant to minimization, (37) can be rewritten as

$$\begin{aligned} &\underset{\mathbf{z}}{\text{minimize}} \ \ -\mathbf{z}^{\mathrm{T}}\mathbf{S}_N\mathbf{z} \\ &\text{subject to } \mathbf{z}^{\mathrm{T}}\mathbf{z} = 1, \quad \mathbf{z}^{\mathrm{T}}\mathbf{1}_N = 0. \end{aligned} \tag{41}$$

Such a problem can be simplified to an eigenvalue problem [58].

Let the Lagrangian function associated with (41) be

$$\mathcal{L}(\mathbf{z}, \mu, \eta) = -\mathbf{z}^{\mathrm{T}}\mathbf{S}_N\mathbf{z} + \mu(\mathbf{z}^T\mathbf{z} - 1) + 2\eta\mathbf{z}^{\mathrm{T}}\mathbf{1}_N, \tag{42}$$

where μ and η are the Lagrange multipliers. The optimal solution $\mathbf{z}^\star$ to (41) satisfies the following necessary conditions:

$$\frac{\partial}{\partial \mathbf{z}}\mathcal{L}(\mathbf{z}^\star, \mu^\star, \eta^\star) = 2\left(-\mathbf{S}_N\mathbf{z}^\star + \mu^\star\mathbf{z}^\star + \eta^\star\mathbf{1}_N\right) = \mathbf{0}, \tag{43}$$

$$\frac{\partial}{\partial \mu}\mathcal{L}(\mathbf{z}^\star, \mu^\star, \eta^\star) = \mathbf{z}^{\star\mathrm{T}}\mathbf{z}^\star - 1 = 0, \tag{44}$$

$$\frac{\partial}{\partial \eta}\mathcal{L}(\mathbf{z}^\star, \mu^\star, \eta^\star) = \mathbf{z}^{\star\mathrm{T}}\mathbf{1}_N = 0. \tag{45}$$

Multiplying (43) on the left by $\mathbf{1}_N^{\mathrm{T}}$, $\eta^\star$ can be calculated as

$$\eta^\star = \frac{1}{N}\mathbf{1}_N^{\mathrm{T}}\mathbf{S}_N\mathbf{z}^\star. \tag{46}$$

Substituting $\eta^\star$ into (43), we obtain

$$\mathbf{T}_N\mathbf{S}_N\mathbf{z}^\star = \mu^\star\mathbf{z}^\star, \tag{47}$$

where $\mathbf{T}_N = \mathbf{I}_N - \frac{1}{N}\mathbf{1}_N\mathbf{1}_N^{\mathrm{T}}$ is the projection matrix onto $\left\{\mathbf{z} \in \mathbb{C}^N \,\middle|\, \mathbf{z}^{\mathrm{T}}\mathbf{1}_N = 0\right\}$. Hence, denoting $\mathbf{K}_N = \mathbf{T}_N\mathbf{S}_N$, the eigenvectors of $\mathbf{K}_N$ are candidates for the solution to the problem (41). Furthermore, since the eigenvectors of $\mathbf{K}_N$ satisfy (44) and (45), multiplying (47) on the left by $\mathbf{z}^{\mathrm{T}}$, we get

$$\begin{aligned} \mathbf{z}^{\mathrm{T}}\mathbf{T}_N\mathbf{S}_N\mathbf{z} &= \mu\mathbf{z}^{\mathrm{T}}\mathbf{z}, \\ \mathbf{z}^{\mathrm{T}}\mathbf{S}_N\mathbf{z} &= \mu. \end{aligned} \tag{48}$$

Therefore, the eigenvector corresponding to the largest eigenvalue μ_0 is the solution to the problem (41). However, finding the eigenvalues of $\mathbf{K}_N$ is numerically ill-conditioned; likewise, $\mathbf{S}_N$. This ill-conditionedness follows from the following fact and proposition.

Fact 1: The eigenvalues of $\mathbf{S}_N$ *are nondegenerate and take values between zero and one. Furthermore, most eigenvalues of* $\mathbf{S}_N$ *are clustered around* 1 *or* 0 *[6].*

Fact 2: Let $\lambda_0, \lambda_1, \ldots, \lambda_{N-1}$ *denote the eigenvalues of* $\mathbf{S}_N$ *such that*

$$1 > \lambda_0 > \lambda_1 > \cdots > \lambda_{N-1} > 0, \tag{49}$$

and their corresponding eigenvectors be $\mathbf{v}_0, \mathbf{v}_1, \ldots, \mathbf{v}_{N-1}$, *whose norm and signs are determined so that*

$$\|\mathbf{v}_k\| = 1, \quad \sum_{n=0}^{N-1} \mathbf{v}_k[n] \geq 0 \ \textit{for } k = 0, 1, \ldots, N-1. \tag{50}$$

The eigenvectors $\mathbf{v}_0, \mathbf{v}_1, \ldots, \mathbf{v}_{N-1}$ *of* $\mathbf{S}_N$ *have the following properties [6]:*

$$\textbf{Orthogonality} : \langle \mathbf{v}_j, \mathbf{v}_k \rangle = 0 \quad \textit{for } j \neq k, \tag{51}$$

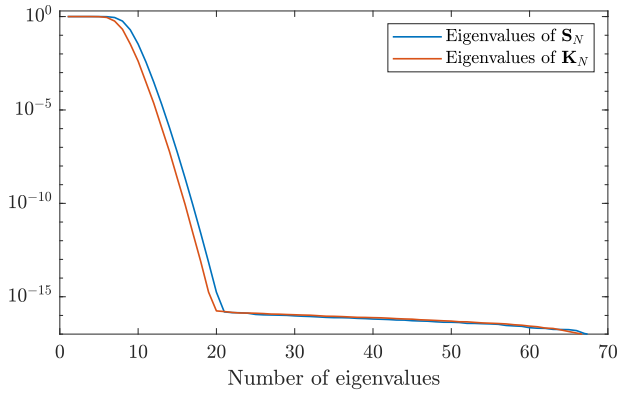

FIGURE 5. Eigenvalues of $\mathbf{S}_N$ and $\mathbf{K}_N$ for $N = 2^7$ and $W = 0.03$.

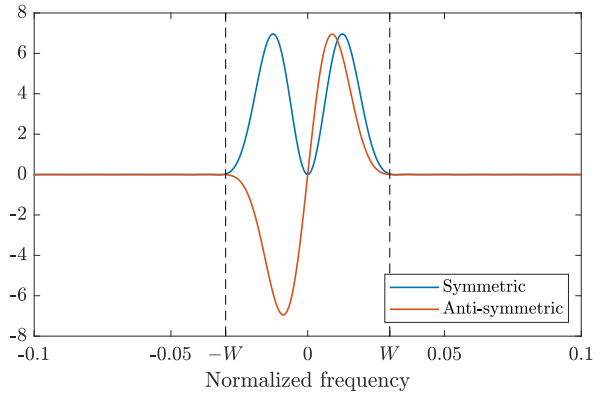

FIGURE 6. Frequency responses $(\mathcal{F}\mathbf{z})(\omega)$ localized in $[-W, W]$ under $\langle \mathbf{z}, \mathbf{1}_N \rangle = 0$ of symmetric and antisymmetric windows. Note that the linear phase of the frequency response is ignored for display.

$$\textbf{Symmetry} : \mathbf{v}_k[n] = (-1)^k \mathbf{v}_k[N-n-1], \tag{52}$$

for $k = 0, 1, \ldots, N-1$.

Proposition 1: $\mathbf{v}_k$ *for* $k = 1, 3, \ldots, 2\lfloor N/2 \rfloor - 1$ *are the eigenvectors of* $\mathbf{K}_N$.

Proof: According to (52), $\mathbf{v}_k$ for $k = 1, 3, \ldots, 2\lfloor N/2 \rfloor - 1$ satisfies

$$\mathbf{T}_N \mathbf{v}_k = \mathbf{v}_k. \tag{53}$$

Then, the following relationship holds:

$$\begin{aligned} \mathbf{K}_N \mathbf{v}_k &= \mathbf{T}_N \mathbf{S}_N \mathbf{v}_k \\ &= \lambda_k \mathbf{T}_N \mathbf{v}_k \\ &= \lambda_k \mathbf{v}_k. \end{aligned} \tag{54}$$

Therefore, λ_k and $\mathbf{v}_k$ are the eigenvalues and eigenvectors of $\mathbf{K}_N$, respectively. □

Finding the eigenvalues of $\mathbf{S}_N$ is numerically ill-conditioned since most eigenvalues of $\mathbf{S}_N$ are clustered around 1 or 0, as shown by the blue line in Fig. 5. Even if the eigenvalues of $\mathbf{S}_N$ are nondegenerate, they behave as if they are degenerate because of rounding errors in the numerical computation. According to Proposition 1, its eigenvalues λ_k for $k = 1, 3, \ldots, 2\lfloor N/2 \rfloor - 1$ are also eigenvalues of $\mathbf{K}_N$. Hence, most eigenvalues of $\mathbf{K}_N$ are also clustered around 1 or 0, as shown by the red line in Fig. 5.

Here, $\mathbf{K}_N$ is centrosymmetric since both $\mathbf{T}_N$ and $\mathbf{S}_N$ are centrosymmetric [59]. Thus, the eigenvectors are symmetric or antisymmetric, but their order is unclear. When $\mathbf{z}$ are symmetric or antisymmetric, $(\mathcal{F}\mathbf{z})(\omega)$ can be represented as the cosine or sine series [60]. Fig. 6 shows $(\mathcal{F}\mathbf{z})(\omega)$ localized in $[-W, W]$ under $\langle \mathbf{z}, \mathbf{1}_N \rangle = 0$. Note that the linear phase of the frequency response is ignored to make the spectrum real-valued for display. The symmetric case contains an extra extremum in $[-W, W]$ compared with the antisymmetric case to satisfy the constraint $\langle \mathbf{z}, \mathbf{1}_N \rangle = 0$. From this observation, the antisymmetric window localizes the frequency response in $[-W, W]$ under the constraint $\langle \mathbf{z}, \mathbf{1}_N \rangle = 0$ more than the symmetric window. Since $\mathbf{v}_k$ for $k = 1, 3, \ldots, 2\lfloor N/2 \rfloor - 1$ are antisymmetric from Proposition 1, the eigenvector $\mathbf{v}_1$ corresponding to the second largest eigenvalue λ_1 is the solution to (37). To compute the eigenvector $\mathbf{v}_1$, efficient methods for computing the eigenvectors of $\mathbf{S}_N$ [61], [62] are available instead of computing the eigenvectors of $\mathbf{K}_N$ directly.

C. CHEBYSHEV WINDOW DERIVATIVE

In this subsection, we consider the design problem of the Chebyshev window derivative. Similar to (37), the direct formulation of the design problem of the Chebyshev window derivative is

$$\begin{aligned} \underset{\mathbf{z}}{\text{minimize}} \quad & \frac{\max_{\omega \in [-\frac{1}{2}, \frac{1}{2}]} \mathcal{W}_W(\omega) |(\mathcal{F}\mathbf{z})(\omega)|}{\max_{\omega \in [-\frac{1}{2}, \frac{1}{2}]} |(\mathcal{F}\mathbf{z})(\omega)|} \\ \text{subject to} \quad & \langle \mathbf{z}, \mathbf{1}_N \rangle = 0. \end{aligned} \tag{55}$$

Considering the constraint $\langle \mathbf{z}, \mathbf{1}_N \rangle = 0$ and the symmetry of the cost function with (37), the solution to (55) should be antisymmetric.

When $\mathbf{z}$ is antisymmetric, the following decomposition of $(\mathcal{F}\mathbf{z})(\omega)$ is proposed by McClellan and Parks [60]:

$$(\mathcal{F}\mathbf{z})(\omega) = \mathrm{e}^{\mathrm{i}(\frac{\pi}{2} - (N-1)\pi\omega)} Q(\omega) P(\omega, \boldsymbol{\alpha}), \tag{56}$$

where

$$P(\omega, \boldsymbol{\alpha}) = \sum_{k=0}^{K-1} \boldsymbol{\alpha}[k] \cos(2\pi\omega k), \tag{57}$$

$$Q(\omega) = \begin{cases} \sin(2\pi\omega), & \text{if } N \text{ is odd} \\ \sin(\pi\omega), & \text{if } N \text{ is even}, \end{cases} \tag{58}$$

$\boldsymbol{\alpha} \in \mathbb{R}^K$, and $K = \lfloor N/2 \rfloor$. The derivation of (56) and the relation between $\boldsymbol{\alpha}$ and $\mathbf{z}$ are explained in Appendix A. The linear phase $\mathrm{e}^{\mathrm{i}(\frac{\pi}{2} - (N-1)\pi\omega)}$ has no effect on the cost function of (55). Since $Q(\omega)P(\omega, \boldsymbol{\alpha})$ is antisymmetric, finding the highest sidelobe level only needs to consider the positive frequency. Furthermore, since the constraint $\langle \mathbf{z}, \mathbf{1}_N \rangle = 0$ is always satisfied when $\mathbf{z}$ is antisymmetric, (55) can be rewritten as

$$\underset{\boldsymbol{\alpha}}{\text{minimize}} \quad \frac{\max_{\omega \in [0, \frac{1}{2}]} \mathcal{W}_W(\omega) |Q(\omega) P(\omega, \boldsymbol{\alpha})|}{\max_{\omega \in [0, \frac{1}{2}]} |Q(\omega) P(\omega, \boldsymbol{\alpha})|}. \tag{59}$$

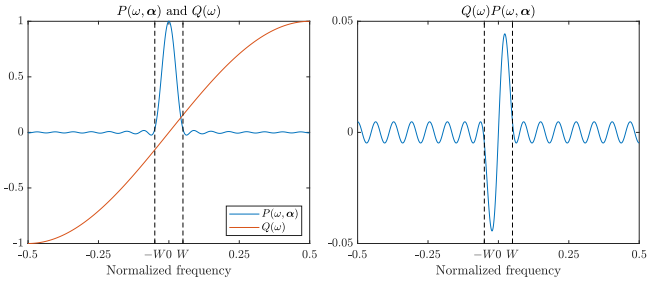

FIGURE 7. $P(\omega,\alpha)$ and $Q(\omega)$ (left) and their product $Q(\omega)P(\omega,\alpha)$ (right).

Fixing the denominator to be 1 as in (41), (59) can be rewritten as

$$\begin{aligned} &\underset{\boldsymbol{\alpha}}{\text{minimize}} \quad \max_{\omega\in[0,\frac{1}{2}]} \mathcal{W}_W(\omega)|Q(\omega)P(\omega,\boldsymbol{\alpha})| \\ &\text{subject to} \quad \max_{\omega\in[0,\frac{1}{2}]} |Q(\omega)P(\omega,\boldsymbol{\alpha})| = 1. \end{aligned} \tag{60}$$

This optimization problem is still difficult to solve due to this equality constraint, hence it needs to be further rewritten. Here, the role of the constraint is to preserve the large peaks of $|Q(\omega)P(\omega,\boldsymbol{\alpha})|$ in $[-W, W]$ while reducing the sidelobe level. Fig. 7 shows $P(\omega,\alpha)$, $Q(\omega)$ and their product $Q(\omega)P(\omega,\boldsymbol{\alpha})$. According to Fig. 7, the peaks of $Q(\omega)P(\omega,\boldsymbol{\alpha})$ in $[-W, W]$ are composed of the product of $Q(\omega)$ and the mainlobe of $P(\omega,\boldsymbol{\alpha})$ in $[-W, W]$. Since $Q(\omega)$ is independent of $\boldsymbol{\alpha}$, constraining $P(0,\boldsymbol{\alpha})$ to a nonzero value will preserve the large peaks of $|Q(\omega)P(\omega,\boldsymbol{\alpha})|$ in $[-W, W]$. Based on these observations, we formulate the design problem of the Chebyshev window derivative as

$$\begin{aligned} &\underset{\boldsymbol{\alpha}}{\text{minimize}} \quad \max_{\omega\in[0,\frac{1}{2}]} \mathcal{W}_W(\omega)|Q(\omega)P(\omega,\boldsymbol{\alpha})| \\ &\text{subject to} \quad P(0,\boldsymbol{\alpha}) = 1. \end{aligned} \tag{61}$$

(61) can be solved using the modified Remez (MRemez) algorithm [63], which is an extension of the Parks–McClellan algorithm [64] to deal with an equality-constrained minimax approximation problem. Introducing a weight function

$$\widetilde{\mathcal{W}}_W^{\epsilon}(\omega) = \begin{cases} \dfrac{1}{\epsilon}, & \text{if } \omega = 0 \\ 0, & \text{if } 0 < |\omega| < W \\ Q(\omega), & \text{if } W \le |\omega|, \end{cases} \tag{62}$$

(61) is rewritten as the unconstrained optimization problem,

$$\underset{\boldsymbol{\alpha}}{\text{minimize}} \quad \max_{\omega\in[0,\frac{1}{2}]} |E(\omega,\boldsymbol{\alpha})|, \tag{63}$$

where

$$E(\omega,\boldsymbol{\alpha}) = \lim_{\epsilon\to 0} \widetilde{\mathcal{W}}_W^{\epsilon}(\omega)\left[P(\omega,\boldsymbol{\alpha}) - D(\omega)\right], \tag{64}$$

$$D(\omega) = \begin{cases} 1, & \text{if } \omega = 0 \\ 0, & \text{if } \omega \ne 0. \end{cases} \tag{65}$$

Denoting the solution of (61) as $\boldsymbol{\alpha}^\star$, there exist $K+1$ frequencies $\omega_0^\star, \omega_1^\star, \ldots, \omega_K^\star$ satisfying $0 = \omega_0^\star < \omega_1^\star < \cdots < \omega_K^\star \le \frac{1}{2}$ such that [65]

$$P(\omega_k^\star,\boldsymbol{\alpha}^\star) = \begin{cases} 1, & \text{if } k = 0 \\ \dfrac{(-1)^k}{\mathcal{W}(\omega_k^\star)}\delta^\star, & \text{if } k = 1\ldots, K \end{cases} \tag{66}$$

where

$$|\delta^\star| = \max_{\omega\in[0,\frac{1}{2}]} |E(\omega,\boldsymbol{\alpha}^\star)|. \tag{67}$$

The MRemez algorithm finds $\omega_0^\star, \omega_1^\star, \ldots, \omega_K^\star$ using the following procedure:

Step 1. Initialize reference frequencies $\omega_0, \omega_1, \ldots, \omega_K$ so that $\omega_0 = 0$ and $W \le \omega_1 < \cdots < \omega_K \le 1/2$.

Step 2. Compute δ and $P(\omega,\boldsymbol{\alpha})$ by the barycentric formula:

$$\delta = \lim_{\epsilon\to 0} \frac{\sum_{k=0}^K \beta_k D(\omega_k)}{\sum_{k=0}^K (-1)^k \beta_k \widetilde{\mathcal{W}}_W^{\epsilon}(\omega_k)}, \tag{68}$$

$$P(\omega,\boldsymbol{\alpha}) = \frac{\sum_{k=0}^K \frac{\beta_k}{\cos(2\pi\omega)-\cos(2\pi\omega_k)} p_k}{\sum_{k=0}^K \frac{\beta_k}{\cos(2\pi\omega)-\cos(2\pi\omega_k)}}, \tag{69}$$

where

$$p_k = \lim_{\epsilon\to 0} D(\omega_k) + \frac{(-1)^k}{\widetilde{\mathcal{W}}_W^{\epsilon}(\omega_k)}\delta, \tag{70}$$

$$\beta_k = \prod_{i=0, i\ne k}^K \frac{1}{\cos(2\pi\omega_k) - \cos(2\pi\omega_i)}. \tag{71}$$

Step 3. Compute $E(\omega,\boldsymbol{\alpha})$ by (64) and find the new reference frequencies $\omega_0^+, \omega_1^+, \ldots, \omega_K^+$ satisfying [66]

$$\operatorname{sign}\left[E(\omega_{k-1}^+,\boldsymbol{\alpha})\right] = -\operatorname{sign}\left[E(\omega_k^+,\boldsymbol{\alpha})\right], \tag{72}$$

$$|\delta| \le |P(\omega_k^+,\boldsymbol{\alpha})|, \tag{73}$$

where at least one of the inequalities is strict.

Step 4. Repeat 2–3 until convergence.

After estimating $\omega_0^\star, \omega_1^\star, \ldots, \omega_K^\star$ using the MRemez algorithm, the Chebyshev window derivative $\mathbf{z}$ can be computed from its frequency response by sampling and performing the inverse DFT,

$$\mathbf{z} = \mathbf{F}^{-1}\hat{\mathbf{z}}, \tag{74}$$

$$\hat{\mathbf{z}}[m] = \mathrm{e}^{\mathrm{i}\left(\frac{\pi}{2} - \frac{N-1}{N}\pi m\right)} Q(m/N)P(m/N,\boldsymbol{\alpha}^\star), \tag{75}$$

for $m = 0, 1, \ldots, N-1$. $P(m/N,\boldsymbol{\alpha}^\star)$ can be calculated from $\omega_0^\star, \omega_1^\star, \ldots, \omega_K^\star$ by the barycentric formula (Step. 2).

D. WINDOW ESTIMATION FROM THE WINDOW DERIVATIVE

In the previous subsections, two window derivatives were introduced as solutions to (36). This subsection presents the method for estimating the window from the obtained window derivative.

Denoting $\mathbf{g}_0 = \mathbf{F}^{-1}\operatorname{diag}(\mathbf{b})\mathbf{F}\mathbf{P}_{L,N}\mathbf{z}$, (34) is rewritten as

$$\mathbf{g} = \mathbf{g}_0 + c\mathbf{1}_L. \tag{76}$$

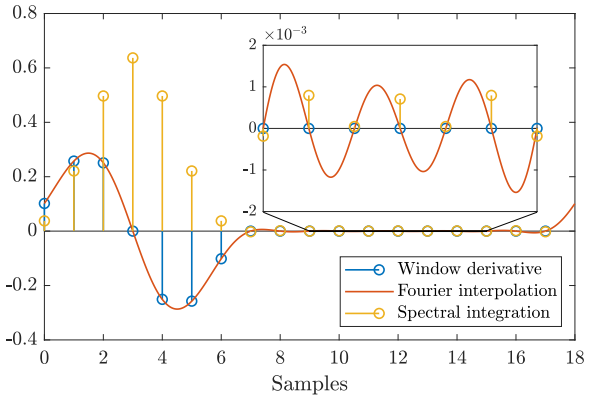

FIGURE 8. Spectral integration of a window derivative supported on $[0, N-1]$ ($N = 7$).

Recall that c is the integral constant, which has to be determined for estimating the window $\mathbf{g}$. In our conference paper [49], estimating c is formulated as the minimization problem of the ratio of the energy outside $[-W, W]$ to the total energy, similar to the Slepian window,

$$\underset{c}{\text{minimize}} \quad 1 - \frac{(\mathbf{g}_0 + c\mathbf{1}_L)^{\mathrm{T}} \mathbf{S}_N (\mathbf{g}_0 + c\mathbf{1}_L)}{(\mathbf{g}_0 + c\mathbf{1}_L)^{\mathrm{T}} (\mathbf{g}_0 + c\mathbf{1}_L)}, \tag{77}$$

to obtain the well-localized frequency response.

An example of the window obtained by the spectral integration from a window derivative supported on $[0, N-1]$ ($N = 7$) is illustrated in Fig. 8. As with the spectral differentiation, even if window derivatives are supported on $[0, N-1]$ ($N < L$), the integrated windows are not supported on $[0, N-1]$. The integrated windows are truncated to have the same support as the window derivatives in practice. This truncation may change the frequency response of the window and decrease the accuracy of the IF computation. In this paper, we propose a method for estimating c based on minimizing the truncation effect.

The truncated window outside $[0, N-1]$ can be expressed using the zero-padding matrix $\mathbf{P}_{L,N}$ as

$$\mathbf{P}_{L,N}\mathbf{P}_{L,N}^{\mathrm{T}}(\mathbf{g}_0 + c\mathbf{1}_L). \tag{78}$$

We estimate c by minimizing the squared error of the window before and after truncation, i.e., our proposed estimation problem is formulated as

$$\underset{c}{\text{minimize}} \quad \frac{1}{2}\left\|(\mathbf{I}_L - \mathbf{P}_{L,N}\mathbf{P}_{L,N}^{\mathrm{T}})(\mathbf{g}_0 + c\mathbf{1}_L)\right\|_2^2. \tag{79}$$

$\mathbf{I}_L - \mathbf{P}_{L,N}\mathbf{P}_{L,N}^{\mathrm{T}}$ can be interpreted as a projection onto the set of vectors that take a zero value in $[0, N-1]$. Note that the cost function of (79) does not go to zero since $\mathbf{g}_0[l]$ outside $[0, N-1]$ oscillates similarly to the spectral differentiation in Fig. 1. This problem is a linear least squares problem, so the solution $c^\star$ to (79) satisfies

$$\mathbf{1}_L^{\mathrm{T}}(\mathbf{I}_L - \mathbf{P}_{L,N}\mathbf{P}_{L,N}^{\mathrm{T}})^{\mathrm{T}}(\mathbf{I}_L - \mathbf{P}_{L,N}\mathbf{P}_{L,N}^{\mathrm{T}})(\mathbf{g}_0 + c^\star\mathbf{1}_L) = 0.$$

Because $\mathbf{I}_L - \mathbf{P}_{L,N}\mathbf{P}_{L,N}^{\mathrm{T}}$ is a diagonal projection matrix and $\mathbf{1}_L^{\mathrm{T}}\left(\mathbf{I}_L - \mathbf{P}_{L,N}\mathbf{P}_{L,N}^{\mathrm{T}}\right)\mathbf{1}_L = L - N$, the solution $c^\star$ to (79) is given by

$$c^\star = -\frac{1}{L-N}\mathbf{1}_L^{\mathrm{T}}(\mathbf{I}_L - \mathbf{P}_{L,N}\mathbf{P}_{L,N}^{\mathrm{T}})\mathbf{g}_0. \tag{80}$$

Since this formulation minimizes the energy of the outer components, the proposed integration method is applicable for the case $N < L$. The proposed integration method is effective when the window width is limited, as in real-time processing, because the effect of truncation can be significant.

V. FREQUENCY RESPONSES OF DESIGNED WINDOWS

This section compares the proposed windows with the Slepian and Dolph–Chebyshev windows. Hereafter, the windows calculated from the Slepian window derivative and the Chebyshev window derivative are referred to as the proposed Slepian window and the proposed Chebyshev window, respectively.

First, Fig. 9 illustrates the shapes and frequency responses of the windows and the window derivatives. The length of the windows was set to $N = 2^7$, and the signal length for the spectral differentiation/integration was set to $L = 2^{12}$. Each parameter W for the window was chosen such that $\omega_{\mathrm{MV}} = 0.03$. Note that the frequency responses in Fig. 9 were normalized such that the maxima are 0 dB. The derivatives of the Slepian and Dolph–Chebyshev windows have nonzero values outside $[0, N-1]$, as in Fig. 1, which are omitted in Figs. 9(c) and (g) since they are too small for illustration. The red lines in Figs. 9(d) and (h) show the frequency responses when these outside values are truncated. Conversely, the proposed Slepian and Chebyshev windows have nonzero values outside $[0, N-1]$ due to the spectral integration. The frequency responses of the truncated windows are plotted as the red lines in Figs. 9(j) and (n).

In the time domain, there is little difference between the shapes of the four windows. The derivative of the Dolph–Chebyshev window (Fig. 9(g)) has a slight oscillation at both ends compared with the others. According to Figs. 9(b) and (l), the Slepian window derivative has a similar sidelobe decay to the Slepian window. Likewise, the sidelobe decay of the Chebyshev window derivative in Fig. 9(f) resembles that of the Dolph–Chebyshev window in Fig. 9(p). Additionally, the proposed Slepian and Chebyshev windows have better sidelobe decays than the Slepian and Dolph–Chebyshev windows, respectively, although their highest sidelobe levels are slightly higher. This is because estimating a window from its derivative window in (34) suppresses the high frequencies. Furthermore, Fig. 9(d), (h), (j), and (n) show that the proposed Slepian and Chebyshev windows have smaller effects on the frequency responses caused by truncation compared with the Slepian and Dolph–Chebyshev windows. The result indicates that the proposed design method can reduce the effect of truncation.

Then, the sidelobe energy and the highest sidelobe level of each window at various bandwidths ω_{MW} are summarized in Fig. 10. Fig. 10 also shows the SE and HSL of four well-known windows: Hann, Blackman, Nuttall, and truncated

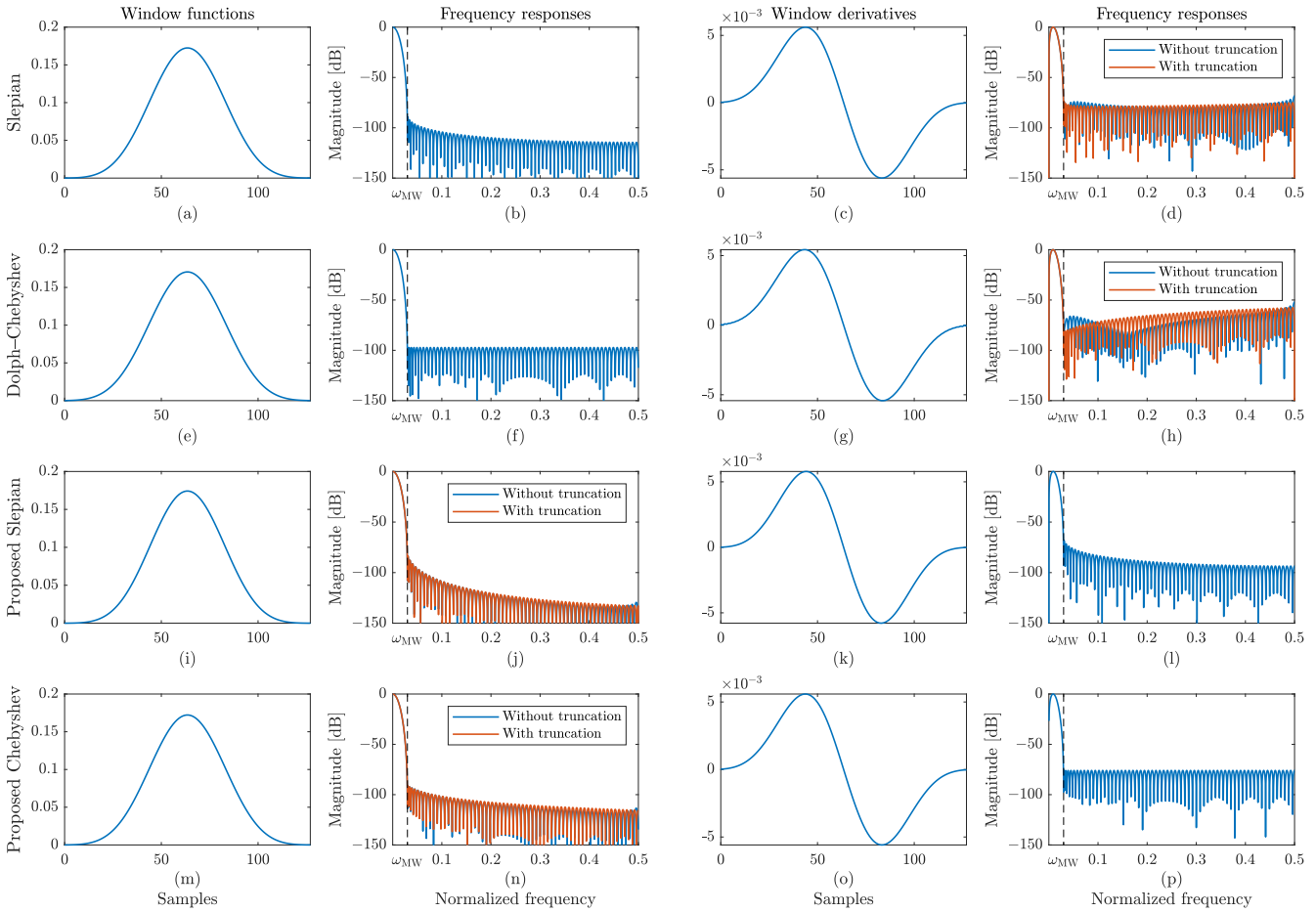

FIGURE 9. Results of designed windows. Each column shows (from left to right) the window functions, their frequency responses, the window derivatives, and the frequency responses of the window derivatives. Each row represents the results of a type of window function. The red lines show the frequency responses when the conventional window derivatives or the proposed windows are truncated outside $[0, N-1]$. The broken black lines indicate the bandwidths ω_{MW}.

Gaussian windows. The truncated Gaussian window is represented by

$$\mathbf{w}_\sigma[n] = \mathrm{e}^{-\frac{\{n-(L-1)/2\}^2}{2\sigma^2}}, \tag{81}$$

where σ is a parameter to control the mainlobe ω_{MW}. Although they were originally defined as continuous functions, we computed these derivatives by the spectral differentiation as mentioned at the end of Sec. II. The jumps in the mainlobe widths seen in the truncated Gaussian and Dolph–Chebyshev are due to nonzero minima in the frequency responses, as shown on the right side of Fig. 11.

When the bandwidth W was set to a higher value, the SE and HSL of the Slepian, Dolph–Chebyshev, proposed Slepian and proposed Chebyshev windows decreased. Fig. 10 confirms that the Slepian window derivative and the Chebyshev window derivative were correctly designed with the desired optimality.

VI. EVALUATION OF IF COMPUTATION

This section compares the four windows in terms of the IF computation. Throughout this section, the window length $N = 2^7$ and the signal length $L = 2^{12}$. Each parameter W for the window was chosen so that $\omega_{\mathrm{MV}} = 0.03$.

A. COMPARING WINDOW INTEGRATION METHODS

First, the proposed integration method in (79) was compared with the conventional estimation method (77) [49]. They were assessed based on the error in computing the IF of the sinusoid in (25).

The frequency responses of the estimated windows from the Slepian and Chebyshev window derivatives using the two integration methods are shown in Fig. 12. The SE and HSL of each window are shown in the upper right corner of each subfigure. Although the conventional method determines c by minimizing the energy outside of $[-W, W]$ to reduce the SE, the frequency responses of the windows estimated by the two methods have comparable SE. However, for both window derivatives, the changes due to truncation of the windows estimated by the proposed method were smaller than those of the conventional method.

The errors of the IF using two integrated windows are shown in Fig. 13. The errors using the conventional method increase due to truncation, but this is not seen in the results of

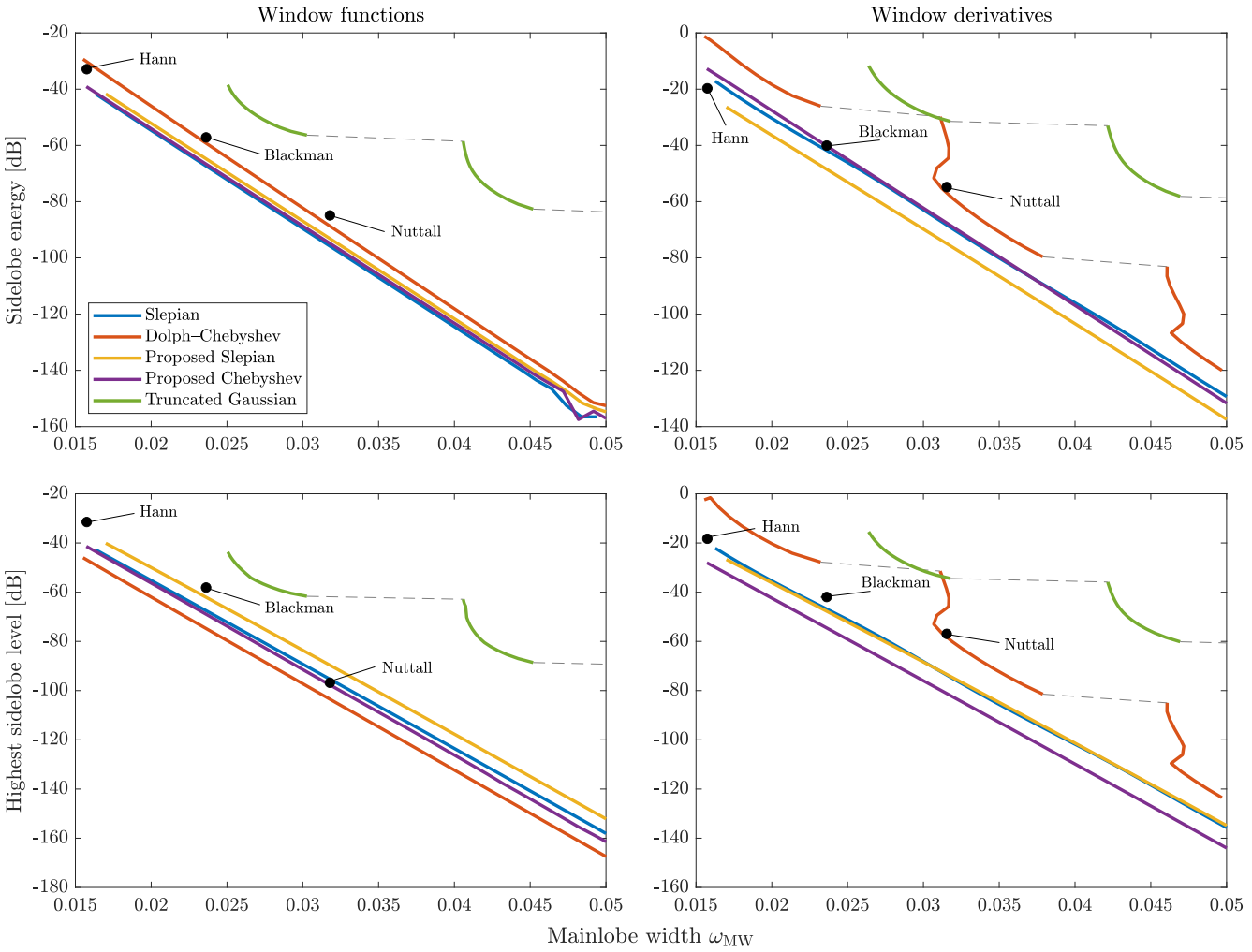

FIGURE 10. Sidelobe energy and highest sidelobe level of designed windows. The top and bottom rows show the sidelobe energy and highest sidelobe level of the window functions, respectively. The left and right columns correspond to the results of the window functions and the window derivatives. Each line color represents a different type of window.

the proposed method. This suggests that the proposed method can estimate the window to avoid an increase in the error due to truncation effects. Additionally, with or without truncation, the errors using the proposed method are smaller than those using the conventional method in $[0, \omega_{\mathrm{MW}}]$. This may be because minimizing the outer energy reduces the oscillation of the frequency responses.

B. COMPARISON OF WINDOWS FOR IF COMPUTATION OF A SINUSOID

Second, the four windows were compared in terms of computing the IF of a sinusoid. They were also evaluated by the error in (26).

The IF errors using the four windows are shown in Fig. 14. Regardless of truncation, the errors using the proposed windows are smaller than those using the conventional windows. In particular, the error using the proposed Chebyshev window was smaller than that using the Slepian window, shown in Fig. 14, even though they have similar frequency responses, shown in Fig. 9. The results indicate that the proposed window design method can improve the accuracy of the IF computation of the sinusoid.

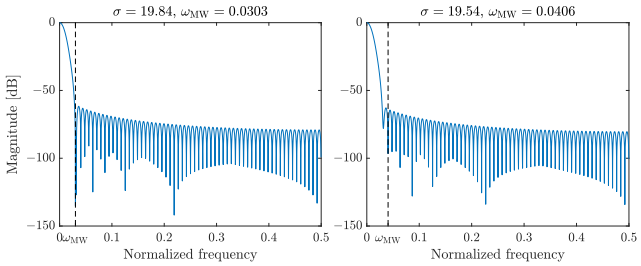

FIGURE 11. Truncated Gaussian windows with different σ.

C. COMPARISON OF WINDOWS FOR IF COMPUTATION IN THE PRESENCE OF ANOTHER SINUSOID

Then, we consider estimating the IF of the sinusoid $\mathbf{s}$ from a signal composed of two complex sinusoids,

$$\mathbf{x} = \mathbf{s} + \boldsymbol{i}, \tag{82}$$

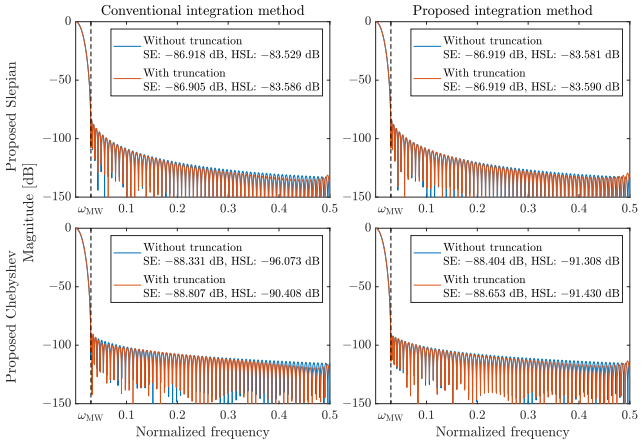

FIGURE 12. Frequency responses of estimated windows from Slepian and Chebyshev window derivatives using two integration methods. The left and right columns correspond to the frequency responses of the conventional and proposed methods, respectively.

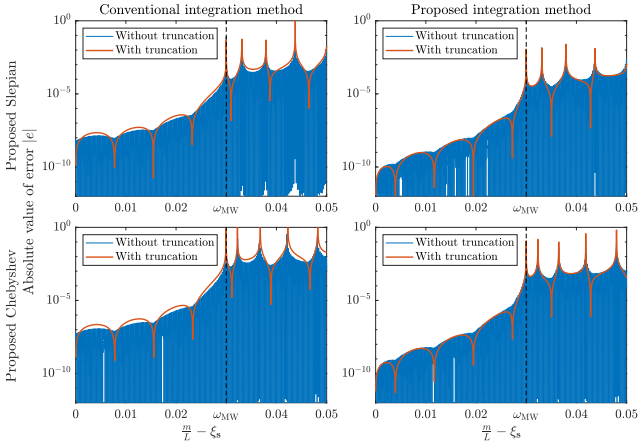

FIGURE 13. IF computation error in a sinusoid using the windows shown in Fig. 12. The left and right columns correspond to the results of the conventional and proposed integration methods, respectively.

where

$$\boldsymbol{i}[l] = A_{\boldsymbol{i}} \mathrm{e}^{\mathrm{i}(2\pi\xi_{\boldsymbol{i}} l + \phi_{\boldsymbol{i}})}, \tag{83}$$

for $l = 0, 1, \ldots, L-1$. $\mathbf{s}$ and $\boldsymbol{i}$ correspond to the target and interference signals, respectively. The IF of $\mathbf{x}$ is expressed as

$$\begin{aligned} &\mathrm{IF}^{\mathbf{x}}_{\mathbf{g}}[n, m] \\ &= -\frac{1}{2\pi} \Im \left\{ \frac{(\mathbf{V}_{\mathbf{g}'}\mathbf{x})[n, m]}{(\mathbf{V}_{\mathbf{g}}\mathbf{x})[n, m]} \right\} \\ &= -\frac{1}{2\pi} \Im \left\{ \frac{r\mathrm{e}^{\mathrm{i}\Delta\phi}(\mathcal{F}\mathbf{g}')(\frac{m}{L} - \xi_{\mathbf{s}}) + (\mathcal{F}\mathbf{g}')(\frac{m}{L} - \xi_{\boldsymbol{i}})}{r\mathrm{e}^{\mathrm{i}\Delta\phi}(\mathcal{F}\mathbf{g})(\frac{m}{L} - \xi_{\mathbf{s}}) + (\mathcal{F}\mathbf{g})(\frac{m}{L} - \xi_{\boldsymbol{i}})} \right\}, \end{aligned} \tag{84}$$

where

$$r = \frac{A_{\mathbf{s}}}{A_{\boldsymbol{i}}}, \qquad \Delta\phi = 2\pi\xi_{\mathbf{s}} n + \phi_{\mathbf{s}} - (2\pi\xi_{\boldsymbol{i}} n + \phi_{\boldsymbol{i}}).$$

The error of the IF between $\mathbf{s}$ and $\mathbf{x}$ is given by

$$e = \mathrm{IF}^{\mathbf{x}}_{\mathbf{g}}[n, m] - \mathrm{IF}^{\mathbf{s}}_{\mathbf{g}}[n, m]$$

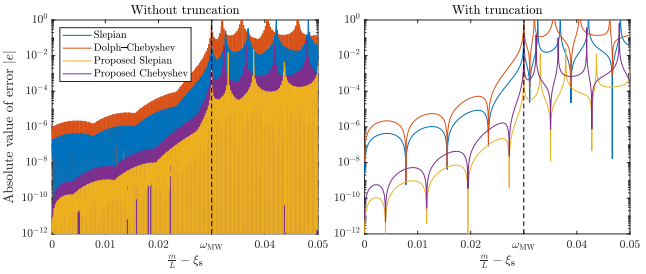

FIGURE 14. IF computation error in a sinusoid using the four windows. The left and right columns correspond to the results without and with truncation, respectively.

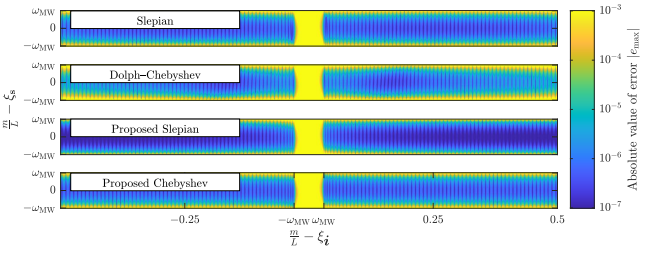

FIGURE 15. IF computation error in the sum of two sinusoids. Each row shows (from top to bottom) the results for the Slepian window, Dolph–Chebyshev window, proposed Slepian window, and proposed Chebyshev window.

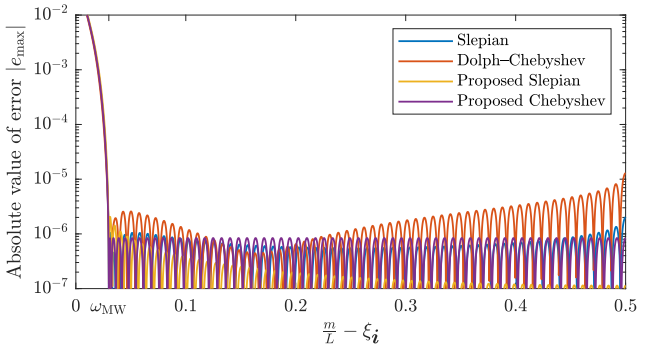

FIGURE 16. Error at $m/L = \xi_{\mathbf{s}}$ in Fig. 15. Each color represents the result of a different window.

$$= -\frac{1}{2\pi} \Im \left\{ \frac{\frac{(\mathcal{F}\mathbf{g}')(\frac{m}{L} - \xi_{\boldsymbol{i}})}{(\mathcal{F}\mathbf{g})(\frac{m}{L} - \xi_{\boldsymbol{i}})} - \frac{(\mathcal{F}\mathbf{g}')(\frac{m}{L} - \xi_{\mathbf{s}})}{(\mathcal{F}\mathbf{g})(\frac{m}{L} - \xi_{\mathbf{s}})}}{r\mathrm{e}^{\mathrm{i}\Delta\phi} \frac{(\mathcal{F}\mathbf{g})(\frac{m}{L} - \xi_{\mathbf{s}})}{(\mathcal{F}\mathbf{g})(\frac{m}{L} - \xi_{\boldsymbol{i}})} + 1} \right\}. \tag{85}$$

According to (12), the real part of the numerator of (85) is zero since the STFT magnitude of a complex sinusoid is time-invariant. Hence, (85) can be rewritten using $\mathrm{IF}^{\boldsymbol{i}}_{\mathbf{g}}$ and $\mathrm{IF}^{\mathbf{s}}_{\mathbf{g}}$ as

$$e = \Re \left\{ \frac{\mathrm{IF}^{\boldsymbol{i}}_{\mathbf{g}}[n, m] - \mathrm{IF}^{\mathbf{s}}_{\mathbf{g}}[n, m]}{r\mathrm{e}^{\mathrm{i}\Delta\phi} \frac{(\mathcal{F}\mathbf{g})(\frac{m}{L} - \xi_{\mathbf{s}})}{(\mathcal{F}\mathbf{g})(\frac{m}{L} - \xi_{\boldsymbol{i}})} + 1} \right\}. \tag{86}$$

The transitions of e associated with the initial phase $\phi_{\mathbf{s}}$, $\phi_{\boldsymbol{i}}$, and the time index n are irrelevant to the evaluation. Moreover, from (25), the IF of a complex sinusoid is constant regardless of the time index n. Therefore, we consider the worst case of e in any $\Delta\phi$. The error e becomes large regardless of sidelobe level when m/L is outside the mainlobe of the target signal or inside the mainlobe of the interference signal. Under these conditions, it is challenging

to obtain a meaningful IF unless the amplitude ratio is quite large. Thus, we consider the case where m/L is inside the mainlobe of the target signal and outside the mainlobe of the interference signal. Assume that the amplitude ratio r satisfies $|(\mathcal{F}\mathbf{g})(m/L-\xi_{\mathbf{s}})/(\mathcal{F}\mathbf{g})(m/L-\xi_{\boldsymbol{i}})| > 1/r$. This assumption is mild in the condition we considered because $|(\mathcal{F}\mathbf{g})(m/L-\xi_{\mathbf{s}})/(\mathcal{F}\mathbf{g})(m/L-\xi_{\boldsymbol{i}})|$ should be large. Then, the worst case of e by choosing $\Delta\phi$ is given by

$$e_{\max} = \frac{\mathrm{IF}^{\boldsymbol{i}}_{\mathbf{g}}[n,m] - \mathrm{IF}^{\mathbf{s}}_{\mathbf{g}}[n,m]}{1 - r\left|\frac{(\mathcal{F}\mathbf{g})(\frac{m}{L}-\xi_{\mathbf{s}})}{(\mathcal{F}\mathbf{g})(\frac{m}{L}-\xi_{\boldsymbol{i}})}\right|}. \tag{87}$$

The deviation of (87) is shown in Appendix B. (87) indicates that as the amplitude ratio r decreases, the error of the IF increases.

Fig. 15 plots the error of the IF computation in (87) for $r = 1$. The bright central areas in the four results correspond to cases where the two mainlobes overlap. The top and bottom bright regions in the four results represent the errors of the IF outside the mainlobe of $\mathbf{s}$. In addition, the error at $m/L = \xi_{\mathbf{s}}$ in Fig. 15 is shown in Fig. 16.

The IF using the Dolph–Chebyshev window had the most significant error among the four windows. In contrast, the results for the proposed Slepian window had the smallest error. The results using the Slepian window and the proposed Chebyshev window had comparable errors. These results suggest that reducing the sidelobe of the window derivative decreases the error of the IF computation.

VII. APPLICATION TO FSST

As an application for IF computation, the proposed windows were applied to the FSSTs of an artificial signal and a speech signal. The FSST of a signal $\mathbf{f}$ with a window function $\mathbf{g}$ is defined as

$$\mathcal{S}^{\mathbf{f}}_{\mathbf{g}}[n,m] := \sum_{k=0}^{L-1} \mathrm{e}^{\mathrm{i}\frac{2\pi kn}{L}} (\mathbf{V}_{\mathbf{g}}\mathbf{f})[n,k]\delta\left[m - \tilde{\mathbf{m}}[n,k]\right], \tag{88}$$

where

$$\tilde{\mathbf{m}}[n,m] := \left\lfloor m + L\cdot \mathrm{IF}^{\mathbf{f}}_{\mathbf{g}}[n,m] \right\rceil, \tag{89}$$

and $\delta[l]$ is the Kronecker delta. We used the Rényi entropy as a metric of the energy concentration of the FSST spectrogram [67]. The Rényi entropy of the FSST spectrogram is given by

$$H_\alpha := \frac{1}{1-\alpha}\log_2\left(\sum_{n,m}\left(\frac{\left|\mathcal{S}^{\mathbf{f}}_{\mathbf{g}}[n,m]\right|}{\sum_{n,m}\left|\mathcal{S}^{\mathbf{f}}_{\mathbf{g}}[n,m]\right|}\right)^{\alpha}\right) - \log_2(L),$$

with $\alpha > 2$ being recommended for the T-F domain measures [67]. $\alpha = 3$ is chosen throughout the experiments.

As shown in Fig. 10, sidelobes can be reduced by increasing the mainlobe width. In contrast, if the mainlobes of multiple components overlap, the IF error becomes large. Therefore, an appropriate mainlobe width must be selected to reduce both effects. The Rényi entropy has also been used as a metric to select the variance of the Gaussian window in STFT and FSST [68], [69]. Since the mainlobe widths of the designed windows will also affect the Rényi entropy of the FSST, we evaluated the Rényi entropy of the FSST for various mainlobe widths.

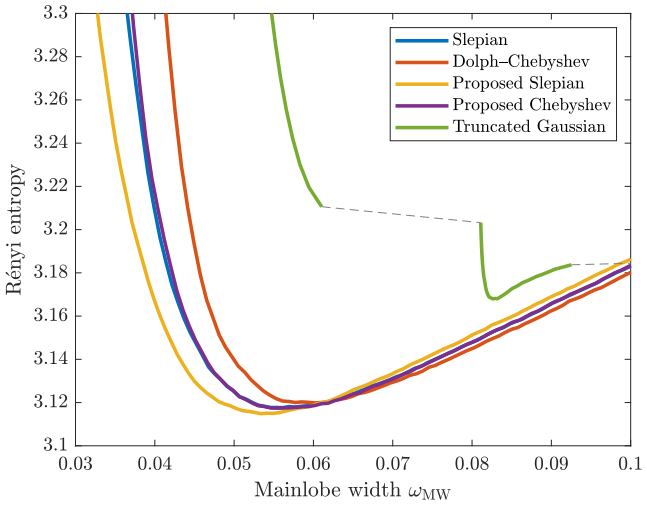

FIGURE 17. Rényi entropies of FSST spectrograms of a synthesized signal.

TABLE 3. Minimum values of the Rényi entropies in Fig. 17 and the corresponding bandwidths.

Window function	Mainlobe width	Rényi entropy
Slepian	0.0562	3.1177
Dolph–Chebyshev	0.0601	3.1198
Proposed Slepian	0.0534	3.1148
Proposed Chebyshev	0.0554	3.1174
Truncated Gaussian	0.0826	3.1680

TABLE 4. Minimum values of the Earth mover's distance in Fig. 18 and the corresponding bandwidths.

Window function	Mainlobe width	Earth mover's distance
Slepian	0.0468	0.6178
Dolph–Chebyshev	0.0505	0.6235
Proposed Slepian	0.0443	0.6144
Proposed Chebyshev	0.0467	0.6178
Truncated Gaussian	0.0594	0.7064

To further evaluate the FSST of an artificial signal, we used the Earth mover's distance [70]. The Earth mover's distance is an index that measures between two distributions and has been used to evaluate the synchrosqueezing-based method [34], [35], [71]. This evaluation consists of averaging the 1D Earth mover's distance between the estimated T-F representation and the ideal representation at each time index n. If the ideal representation is known, the Earth mover's distance is a more valid metric for estimating the T-F representation than the Rényi entropy.

A. FSST OF ARTIFICIAL SIGNALS

The proposed windows were evaluated with the FSST of a real-valued artificial signal, which contained a sinusoid, a linear chirp, and a quadratic chirp. The window length was

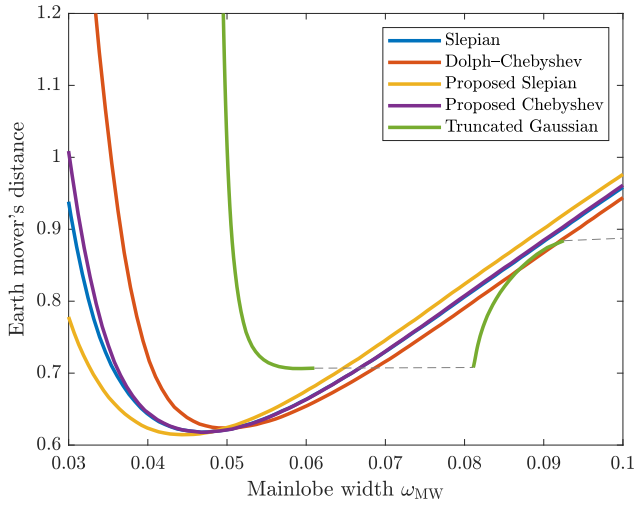

FIGURE 18. Earth mover's distance of FSST spectrograms of a synthesized signal.

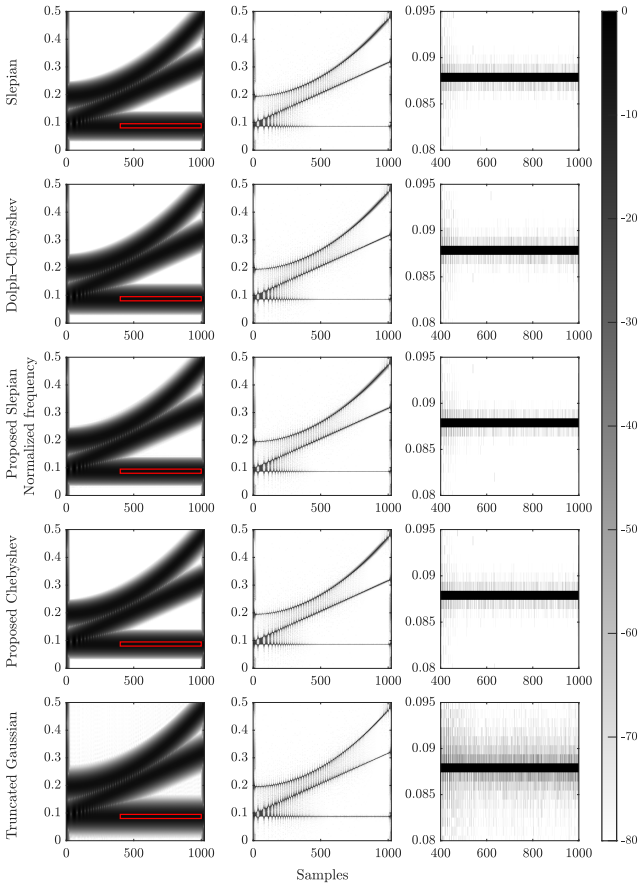

FIGURE 19. FSST spectrograms of an artificial signal. Each column shows (from left to right) the spectrograms, FSST spectrograms, and enlargements of the FSST spectrograms in the red box. Each row shows (from top to bottom) the results for the Slepian, Dolph–Chebyshev, proposed Slepian, proposed Chebyshev, and truncated Gaussian windows.

set to $N = 2^6$ because the calculation of the Rényi entropy of FSST was numerically unstable when $N = 2^7$.

The Rényi entropies of the FSST with different mainlobe widths ω_{MW} are plotted in Fig. 17. Table 3 shows

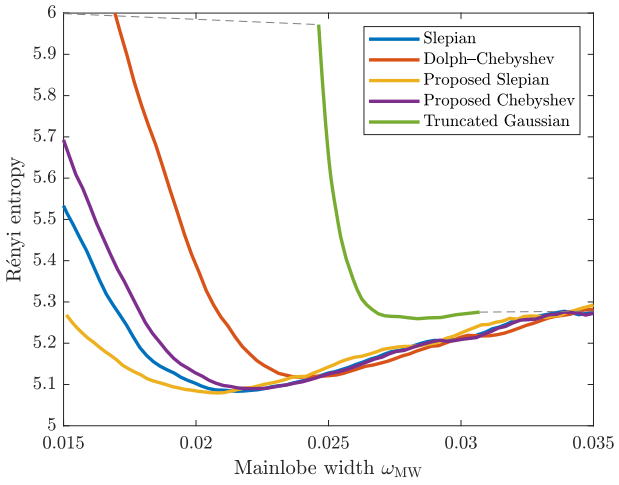

FIGURE 20. Rényi entropies of FSST spectrograms of a speech signal.

the minimum values of the Rényi entropies in Fig. 17 and the corresponding bandwidths. Compared to the other four windows, the widely used truncated Gaussian window shows poor performance. The Slepian window and the proposed Chebyshev window show approximately equivalent performance. The proposed Slepian window achieves the best performance among the five windows. Then, the Earth mover's distance of FSST with different mainlobe widths ω_{MW} are shown in Fig. 18, and their minimum values are shown in Table 4. Although the mainlobe widths that obtain the minima are different, the FSST spectrogram using the proposed Slepian has the smallest distance. These results indicate that the proposed Slepian window provides the most concentrated FSST spectrogram of the five windows.

Fig. 19 illustrates the T-F representations obtained by the STFT and FSST in the case of Table 3. Focusing on the enlargement in the red box (the right column of Fig. 19), it can be confirmed that the component outside the center frequency is reduced using the proposed Slepian window. The FSST spectrogram using the proposed Chebyshev window is almost as sharp as that using the Slepian window.

B. FSST OF SPEECH SIGNAL

We considered a speech signal with a sampling frequency of 7,418 Hz. The window length was set to $N = 2^7$. Since the ideal T-F representation is unknown, the Earth mover's distance cannot be used for evaluation, and only the Rényi entropy is used in this experiment.

Fig. 20 and Table 5 show Rényi entropies of SST with different bandwidths and their minimum values, respectively. As in the case of the synthesized signal, FSST with the proposed Slepian window achieves the best performance in terms of the Rényi entropy. Fig. 21 depicts the T-F representations obtained by the STFT and FSST in the case of Table 5. Although the appearances of the spectrograms are similar, the proposed Slepian window provides the sharpest FSST spectrogram of the four windows. The results confirmed that the proposed Slepian window provides the sharpest FSST

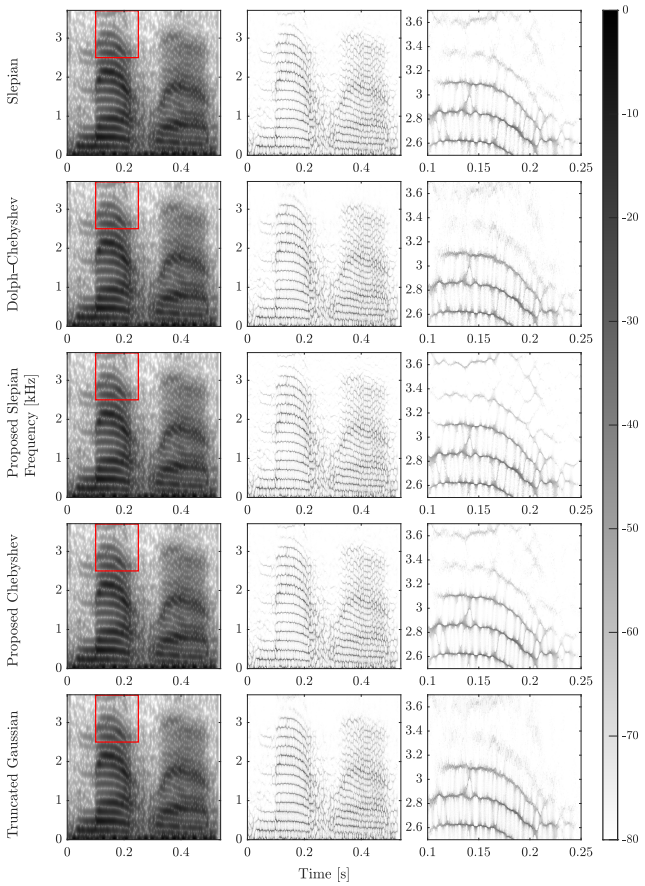

FIGURE 21. FSST spectrograms of a speech signal. Each column shows (from left to right) the spectrograms, FSST spectrograms, and enlargements of the FSST spectrograms in the red box. Each row shows (from top to bottom) the results for the Slepian, Dolph–Chebyshev, proposed Slepian, proposed Chebyshev, and truncated Gaussian windows.

TABLE 5. Minimum values of the Rényi entropies in Fig. 20 and the corresponding bandwidths.

Window function	Mainlobe width	Rényi entropy
Slepian	0.0215	5.0835
Dolph–Chebyshev	0.0239	5.1175
Proposed Slepian	0.0208	5.0794
Proposed Chebyshev	0.0221	5.0899
Truncated Gaussian	0.0284	5.2594

spectrogram of the four windows for a real speech signal as well.

The proposed Slepian window showed the best performance throughout the experiments in this section. Therefore, the proposed Slepian window can be useful for FSST applications. However, the proposed Chebyshev window may be preferable depending on the signal of interest because the sidelobes of the Chebyshev window derivative near the mainlobe are smaller than those of the Slepian window derivative.

VIII. CONCLUSION

In this paper, we proposed a framework to design a window function for the IF computation. The proposed method first designs the window derivative to minimize the sidelobes and then estimates the window function from the designed window derivative. We designed two minimum-sidelobe derivatives to minimize the SE and HSL, referred to as the Slepian and Chebyshev window derivatives, respectively. The integral constant that appears when integrating the designed window derivative is estimated to minimize the truncation effect. In the IF computation of a sinusoid, the proposed windows reduce the error compared to certain other windows. In addition, the proposed Slepian window showed the best performance in the FSST among the several windows.

Some phase-aware techniques use not only the IF but also the group delay and higher-order derivatives of the phase [33]–[35]. Moreover, phase derivatives also play an important role in wavelet synchrosqueezing transform and other filterbank-based methods. Therefore, future work will include generalizing the proposed method to these elements and investigating the method's computational efficiency.

APPENDIX A
TRIGONOMETRIC REPRESENTATION OF THE FREQUENCY RESPONSE OF THE WINDOW DERIVATIVE

This appendix explains the derivation of (56) and the relation between $\boldsymbol{\alpha}$ and $\mathbf{z}$ based on [60]. The frequency response of the antisymmetric window $\mathbf{z}$ can be represented as a sine series. When N is odd,

$$(\mathcal{F}\mathbf{z})(\omega) = \mathrm{e}^{\mathrm{i}\left(\frac{\pi}{2}-(N-1)\pi\omega\right)} \sum_{k=1}^{K} \mathbf{a}[k] \sin(2\pi\omega k), \tag{90}$$

where $K = (N-1)/2$ and $\mathbf{a}[k] = 2\mathbf{z}[K-k]$ for $k = 1, \ldots, K$, and $\mathbf{z}[K] = 0$. When N is even,

$$(\mathcal{F}\mathbf{z})(\omega) = \mathrm{e}^{\mathrm{i}\left(\frac{\pi}{2}-(N-1)\pi\omega\right)} \sum_{k=1}^{K} \mathbf{a}[k] \sin\left(2\pi\omega\left(k-\frac{1}{2}\right)\right) \tag{91}$$

where $K = N/2$ and $\mathbf{a}[k] = 2\mathbf{z}[K-k]$ for $k = 1, \ldots, K$. (90) and (91) can be rewritten as a cosine series using the trigonometric identities,

$$\cos\theta_1 \cos\theta_2 = \frac{1}{2}\left[\cos(\theta_1+\theta_2) + \cos(\theta_1-\theta_2)\right], \tag{92}$$

$$\cos\theta_1 \sin\theta_2 = \frac{1}{2}\left[\sin(\theta_1+\theta_2) - \sin(\theta_1-\theta_2)\right]. \tag{93}$$

When window length N is odd,

$$\sum_{k=1}^{K} \mathbf{a}[k] \sin(2\pi\omega k) = \sin(2\pi\omega) \sum_{k=0}^{K-1} \boldsymbol{\alpha}[k] \cos(2\pi\omega k), \tag{94}$$

where

$$\mathbf{a}[k] = \begin{cases} \boldsymbol{\alpha}[0] - \frac{1}{2}\boldsymbol{\alpha}[2], & \text{if } k = 1 \\ \frac{1}{2}(\boldsymbol{\alpha}[k-1] - \boldsymbol{\alpha}[k+1]), & \text{if } k = 2, 3, \ldots, K-2 \\ \frac{1}{2}\boldsymbol{\alpha}[k-1], & \text{if } k = K-1, K. \end{cases} \tag{95}$$

When window length N is even,

$$\sum_{k=1}^{K} \mathbf{a}[k] \sin\left(2\pi\omega\left(k-\frac{1}{2}\right)\right) = \sin(\pi\omega) \sum_{k=0}^{K-1} \boldsymbol{\alpha}[k] \cos(2\pi\omega k), \quad (96)$$

where

$$\mathbf{a}[k] = \begin{cases} \boldsymbol{\alpha}[0] - \frac{1}{2}\boldsymbol{\alpha}[1], & \text{if } k = 1 \\ \frac{1}{2}(\boldsymbol{\alpha}[k-1] - \boldsymbol{\alpha}[k]), & \text{if } k = 2, 3, \ldots, K-1 \\ \frac{1}{2}\boldsymbol{\alpha}[k-1], & \text{if } k = K. \end{cases} \quad (97)$$

Hence, using (57) and (58), $(\mathcal{F}\mathbf{z})(\omega)$ in the odd and even cases can be uniformly rewritten as

$$(\mathcal{F}\mathbf{z})(\omega) = \mathrm{e}^{\mathrm{i}\left(\frac{\pi}{2} - (N-1)\pi\omega\right)} Q(\omega) P(\omega, \boldsymbol{\alpha}), \quad (98)$$

which equals (56).

After obtaining the solution $\boldsymbol{\alpha}^\star$ by solving (61), the window derivative $\mathbf{z}$ is calculated using (95) and

$$\mathbf{z}[n] = \begin{cases} \frac{1}{2}\mathbf{a}[K-n], & \text{for } n = 0, \ldots, K-1 \\ 0 & \text{for } n = K \\ -\frac{1}{2}\mathbf{a}[n-K], & \text{for } n = K+1, \ldots, N-1 \end{cases} \quad (99)$$

when N is odd, and (97) and

$$\mathbf{z}[n] = \begin{cases} \frac{1}{2}\mathbf{a}[K-n], & \text{for } n = 0, \ldots, K-1 \\ -\frac{1}{2}\mathbf{a}[n-K], & \text{for } n = K, \ldots, N-1 \end{cases} \quad (100)$$

when N is even.

APPENDIX B
DERIVATION OF (87)

Let $\rho \in \mathbb{R}_+$ and $\varphi \in (-\pi, \pi]$ such that

$$r\mathrm{e}^{\mathrm{i}\Delta\phi} \frac{(\mathcal{F}\mathbf{g})(m/L - \xi_\mathbf{s})}{(\mathcal{F}\mathbf{g})(m/L - \xi_\mathbf{i})} =: \rho\mathrm{e}^{\mathrm{i}\varphi}. \quad (101)$$

Then, (85) can be rewritten as

$$e = \Re\left\{\frac{(\mathrm{IF}^{\mathbf{i}}_{\mathbf{g}}[n,m] - \mathrm{IF}^{\mathbf{s}}_{\mathbf{g}}[n,m])(\rho\mathrm{e}^{-\mathrm{i}\varphi} + 1)}{(\rho\mathrm{e}^{\mathrm{i}\varphi} + 1)(\rho\mathrm{e}^{-\mathrm{i}\varphi} + 1)}\right\}. \quad (102)$$

Since $\mathrm{IF}^{\mathbf{s}}_{\mathbf{g}}$ and $\mathrm{IF}^{\mathbf{i}}_{\mathbf{g}}$ are real,

$$e = \frac{(\mathrm{IF}^{\mathbf{i}}_{\mathbf{g}}[n,m] - \mathrm{IF}^{\mathbf{s}}_{\mathbf{g}}[n,m])(\rho\cos\varphi + 1)}{\rho^2 + 2\rho\cos\varphi + 1}. \quad (103)$$

When e becomes extrema, φ must satisfy

$$\frac{\partial e}{\partial \varphi} = \frac{(\mathrm{IF}^{\mathbf{i}}_{\mathbf{g}}[n,m] - \mathrm{IF}^{\mathbf{s}}_{\mathbf{g}}[n,m])\rho(1-\rho^2)\sin\varphi}{(\rho^2 + 2\rho\cos\varphi + 1)^2} = 0. \quad (104)$$

Because we assumed that $|(\mathcal{F}\mathbf{g})(m/L - \xi_\mathbf{s})/(\mathcal{F}\mathbf{g})(m/L - \xi_\mathbf{i})| > 1/r$, ρ must be greater than 1. Thus, the denominator of (104) is not zero, and $\frac{\partial e}{\partial \varphi}$ becomes zero if $\varphi = 0$ or $\varphi = \pi$. Substituting $\varphi = 0$ or $\varphi = \pi$ for (102),

$$e_0 = \frac{(\mathrm{IF}^{\mathbf{i}}_{\mathbf{g}}[n,m] - \mathrm{IF}^{\mathbf{s}}_{\mathbf{g}}[n,m])(\rho+1)}{\rho^2 + 2\rho + 1} = \frac{\mathrm{IF}^{\mathbf{i}}_{\mathbf{g}}[n,m] - \mathrm{IF}^{\mathbf{s}}_{\mathbf{g}}[n,m]}{1+\rho}, \quad (105)$$

$$e_\pi = \frac{(\mathrm{IF}^{\mathbf{i}}_{\mathbf{g}}[n,m] - \mathrm{IF}^{\mathbf{s}}_{\mathbf{g}}[n,m])(-\rho+1)}{\rho^2 - 2\rho + 1} = \frac{\mathrm{IF}^{\mathbf{i}}_{\mathbf{g}}[n,m] - \mathrm{IF}^{\mathbf{s}}_{\mathbf{g}}[n,m]}{1-\rho}. \quad (106)$$

The difference between the squares of these is

$$e_0^2 - e_\pi^2 = (\mathrm{IF}^{\mathbf{i}}_{\mathbf{g}}[n,m] - \mathrm{IF}^{\mathbf{s}}_{\mathbf{g}}[n,m])^2 \left\{\frac{1}{(1+\rho)^2} + \frac{1}{(1-\rho)^2}\right\} = (\mathrm{IF}^{\mathbf{i}}_{\mathbf{g}}[n,m] - \mathrm{IF}^{\mathbf{s}}_{\mathbf{g}}[n,m])^2 \frac{-4\rho}{(1-\rho^2)^2} < 0.$$

Hence, the worst-case error is e_π, and e_π is equal to (87) by substituting $\rho = r\,|(\mathcal{F}\mathbf{g})(m/L - \xi_\mathbf{s})/(\mathcal{F}\mathbf{g})(m/L - \xi_\mathbf{i})|$.

REFERENCES

[1] D. Gabor, "Theory of communication. Part 1: The analysis of information," *J. Inst. Elect. Eng.*, vol. 93, no. 26, pp. 429–441, Jul. 1946.
[2] H. G. Feichtinger and T. Strohmer, Eds., *Gabor Analysis and Algorithms*. Boston, MA, USA: Birkhäuser, 1998.
[3] K. Gröchenig, *Foundations of Time-Frequency Analysis*. Boston, MA, USA: Birkhäuser, 2001.
[4] B. Boashash, *Time-Frequency Signal Analysis and Processing: A Comprehensive Reference*, 2nd ed. London, U.K.: Academic, 2016.
[5] C. L. Dolph, "A current distribution for broadside arrays which optimizes the relationship between beam width and side-lobe level," *Proc. IRE*, vol. 34, no. 6, pp. 335–348, Jun. 1946.
[6] D. Slepian, "Prolate spheroidal wave functions, Fourier analysis, and uncertainty-V: The discrete case," *Bell Syst. Tech. J.*, vol. 57, no. 5, pp. 1371–1430, May 1978.
[7] F. J. Harris, "On the use of windows for harmonic analysis with the discrete Fourier transform," *Proc. IEEE*, vol. 66, no. 1, pp. 51–83, Jan. 1978.
[8] J. Kaiser and R. Schafer, "On the use of the I_0-sinh window for spectrum analysis," *IEEE Trans. Acoust., Speech, Signal Process.*, vol. ASSP-28, no. 1, pp. 105–107, Feb. 1980.
[9] T. Saramäki, "A class of window functions with nearly minimum sidelobe energy for designing FIR filters," in *Proc. IEEE Int. Symp. Circuits Syst. (ISCAS)*, vol. 1, May 1989, pp. 359–362.
[10] S. W. Bergen and A. Antoniou, "Generation of ultraspherical window functions," in *Proc. Eur. Signal Process. Conf. (EUSIPCO)*, 2002, pp. 1–4.
[11] S. W. A. Bergen and A. Antoniou, "Design of ultraspherical window functions with prescribed spectral characteristics," *EURASIP J. Adv. Signal Process.*, vol. 2004, no. 13, pp. 2053–2065, Dec. 2004.
[12] K. Avci and A. Nacaroglu, "Cosh window family and its application to FIR filter design," *AEU-Int. J. Electron. Commun.*, vol. 63, no. 11, pp. 907–916, Nov. 2009.
[13] A. H. Nuttall, "Some windows with very good sidelobe behavior," *IEEE Trans. Acoust., Speech, Signal Process.*, vol. ASSP-29, no. 1, pp. 84–91, Feb. 1981.
[14] H. Kawahara, K.-I. Sakakibara, M. Morise, H. Banno, T. Toda, and T. Irino, "A new cosine series antialiasing function and its application to aliasing-free glottal source models for speech and singing synthesis," in *Proc. Annu. Conf. Int. Speech. Commun. Assoc. (INTERSPEECH)*, Aug. 2017, pp. 1358–1362.
[15] Z. Cvetkovic, "On discrete short-time Fourier analysis," *IEEE Trans. Signal Process.*, vol. 48, no. 9, pp. 2628–2640, Sep. 2000.

[16] M. R. Wilbur, T. N. Davidson, and J. P. Reilly, "Efficient design of oversampled NPR GDFT filterbanks," *IEEE Trans. Signal Process.*, vol. 52, no. 7, pp. 1947–1962, Jun. 2004.

[17] T. Werther, Y. C. Eldar, and N. K. Subbanna, "Dual Gabor frames: Theory and computational aspects," *IEEE Trans. Signal Process.*, vol. 53, no. 11, pp. 4147–4158, Nov. 2005.

[18] J. Jiang, S. Ouyang, and F. Zhou, "Design of NPR DFT-modulated filter banks via iterative updating algorithm," *Circuits, Syst., Signal Process.*, vol. 32, no. 3, pp. 1351–1362, Jun. 2013.

[19] N. Perraudin, N. Holighaus, P. L. Søndergaard, and P. Balazs, "Designing Gabor windows using convex optimization," *Appl. Math. Comput.*, vol. 330, pp. 266–287, Aug. 2018.

[20] T. Kusano, Y. Masuyama, K. Yatabe, and Y. Oikawa, "Designing nearly tight window for improving time-frequency masking," in *Proc. Int. Congr. Acoust. (ICA)*, Sep. 2019, pp. 2885–2892.

[21] F. Auger, P. Flandrin, Y.-T. Lin, S. McLaughlin, S. Meignen, T. Oberlin, and H.-T. Wu, "Time-frequency reassignment and synchrosqueezing: An overview," *IEEE Signal Process. Mag.*, vol. 30, no. 6, pp. 32–41, Nov. 2013.

[22] K. Kodera, C. De Villedary, and R. Gendrin, "A new method for the numerical analysis of non-stationary signals," *Phys. Earth Planet. Interiors*, vol. 12, nos. 2–3, pp. 142–150, Aug. 1976.

[23] F. Auger and P. Flandrin, "Improving the readability of time-frequency and time-scale representations by the reassignment method," *IEEE Trans. Signal Process.*, vol. 43, no. 5, pp. 1068–1089, May 1995.

[24] S. Fenet, R. Badeau, and G. Richard, "Reassigned time–frequency representations of discrete time signals and application to the constant-Q transform," *Signal Process.*, vol. 132, pp. 170–176, Mar. 2017.

[25] N. Holighaus, Z. Průša, and P. L. Søndergaard, "Reassignment and synchrosqueezing for general time–frequency filter banks, subsampling and processing," *Signal Process.*, vol. 125, pp. 1–8, Aug. 2016.

[26] I. Daubechies and S. Maes, "A nonlinear squeezing of the continuous wavelet transform based on auditory nerve models," in *Wavelets in Medicine and Biology*, A. Aldroubi and M. A. Unser, Eds. Boca Raton, FL, USA: CRC Press, 1996, pp. 527–546.

[27] I. Daubechies, J. Lu, and H. T. Wu, "Synchrosqueezed wavelet transforms: An empirical mode decomposition-like tool," *Appl. Comput. Harmon. Anal.*, vol. 30, no. 2, pp. 243–261, Mar. 2011.

[28] G. Thakur and H.-T. Wu, "Synchrosqueezing-based recovery of instantaneous frequency from nonuniform samples," *SIAM J. Math. Anal.*, vol. 43, no. 5, pp. 2078–2095, Sep. 2011.

[29] T. Oberlin, S. Meignen, and V. Perrier, "The Fourier-based synchrosqueezing transform," in *Proc. IEEE Int. Conf. Acoust., Speech Signal Process. (ICASSP)*, May 2014, pp. 315–319.

[30] Z.-L. Huang, J. Zhang, T.-H. Zhao, and Y. Sun, "Synchrosqueezing S-transform and its application in seismic spectral decomposition," *IEEE Trans. Geosci. Remote Sens.*, vol. 54, no. 2, pp. 817–825, Feb. 2016.

[31] S. Meignen, T. Oberlin, and S. McLaughlin, "A new algorithm for multicomponent signals analysis based on synchrosqueezing: With an application to signal sampling and denoising," *IEEE Trans. Signal Process.*, vol. 60, no. 11, pp. 5787–5798, Nov. 2012.

[32] G. Thakur, E. Brevdo, N. S. Fučkar, and H. T. Wu, "The synchrosqueezing algorithm for time-varying spectral analysis: Robustness properties and new paleoclimate applications," *Signal Process.*, vol. 93, no. 5, pp. 1079–1094, May 2013.

[33] T. Oberlin, S. Meignen, and V. Perrier, "Second-order synchrosqueezing transform or invertible reassignment? Towards ideal time-frequency representations," *IEEE Trans. Signal Process.*, vol. 63, no. 5, pp. 1335–1344, Mar. 2015.

[34] D.-H. Pham and S. Meignen, "High-order synchrosqueezing transform for multicomponent signals analysis—With an application to gravitational-wave signal," *IEEE Trans. Signal Process.*, vol. 65, no. 12, pp. 3168–3178, Jun. 2017.

[35] R. Behera, S. Meignen, and T. Oberlin, "Theoretical analysis of the second-order synchrosqueezing transform," *Appl. Comput. Harmon. Anal.*, vol. 45, pp. 379–404, Sep. 2018.

[36] J. L. Flanagan and R. M. Golden, "Phase vocoder," *Bell Syst. Tech. J.*, vol. 45, no. 9, pp. 1493–1509, Nov. 1966.

[37] M. Dolson, "The phase vocoder: A tutorial," *Comput. Music J.*, vol. 10, no. 4, pp. 14–27, 1986.

[38] S. S. Abeysekera and K. P. Padhi, "An investigation of window effects on the frequency estimation using the phase vocoder," *IEEE Trans. Audio, Speech, Language Process.*, vol. 14, no. 4, pp. 1432–1439, Jul. 2006.

[39] M. Betser, P. Collen, G. Richard, and B. David, "Estimation of frequency for AM/FM models using the phase vocoder framework," *IEEE Trans. Signal Process.*, vol. 56, no. 2, pp. 505–517, Feb. 2008.

[40] A. Hiruma, K. Yatabe, and Y. Oikawa, "Separating stereo audio mixture having, no., phase difference by convex clustering and disjointness map," in *Proc. Int. Workshop Acoust. Signal Enhancement (IWAENC)*, Sep. 2018, pp. 266–270.

[41] A. Hiruma, K. Yatabe, and Y. Oikawa, "Detection of clean time-frequency bins based on phase derivative of multichannel signals," in *Proc. Int. Congr. Acoust. (ICA)*, Sep. 2019, pp. 2797–2804.

[42] K. Yatabe and Y. Oikawa, "Phase corrected total variation for audio signals," in *Proc. IEEE Int. Conf. Acoust., Speech Signal Process. (ICASSP)*, Apr. 2018, pp. 656–660.

[43] Y. Masuyama, K. Yatabe, and Y. Oikawa, "Phase-aware harmonic/percussive source separation via convex optimization," in *Proc. IEEE Int. Conf. Acoust., Speech Signal Process. (ICASSP)*, May 2019, pp. 985–989.

[44] Y. Masuyama, K. Yatabe, and Y. Oikawa, "Low-rankness of complex-valued spectrogram and its application to phase-aware audio processing," in *Proc. IEEE Int. Conf. Acoust., Speech Signal Process. (ICASSP)*, May 2019, pp. 855–859.

[45] K. Yatabe, Y. Masuyama, T. Kusano, and Y. Oikawa, "Representation of complex spectrogram via phase conversion," *Acoust. Sci. Technol.*, vol. 40, no. 3, pp. 170–177, 2019.

[46] A. P. Stark and K. K. Paliwal, "Speech analysis using instantaneous frequency deviation," in *Proc. Annu. Conf. Int. Speech. Commun. Assoc. (INTERSPEECH)*, Sep. 2008, pp. 2602–2605.

[47] M. Grimaldi and F. Cummins, "Speaker identification using instantaneous frequencies," *IEEE Trans. Audio, Speech, Language Process.*, vol. 16, no. 6, pp. 1097–1111, Aug. 2008.

[48] A. Gaich and P. Mowlaee, "On speech quality estimation of phase-aware single-channel speech enhancement," in *Proc. IEEE Int. Conf. Acoust., Speech Signal Process. (ICASSP)*, Apr. 2015, pp. 216–220.

[49] T. Kusano, K. Yatabe, and Y. Oikawa, "Maximally energy-concentrated differential window for phase-aware signal processing using instantaneous frequency," in *Proc. IEEE Int. Conf. Acoust., Speech Signal Process. (ICASSP)*, May 2020, pp. 5825–5829.

[50] B. Boashash, "Estimating and interpreting the instantaneous frequency of a signal. I. Fundamentals," *Proc. IEEE*, vol. 80, no. 4, pp. 520–538, Apr. 1992.

[51] B. Boashash, "Estimating and interpreting the instantaneous frequency of a signal. II. Algorithms and applications," *Proc. IEEE*, vol. 80, no. 4, pp. 540–568, Apr. 1992.

[52] N. Perraudin, N. Holighaus, P. Majdak, and P. Balazs, "Inpainting of long audio segments with similarity graphs," *IEEE/ACM Trans. Audio, Speech, Language Process.*, vol. 26, no. 6, pp. 1083–1094, Jun. 2018.

[53] P. Flandrin, F. Auger, and E. Chassande-Mottin, "Time-frequency reassignment: From principles to algorithms," in *Applications in Time-Frequency Signal Processing*, A. Papandreou-Suppappola, Ed., 1st ed. Boca Raton, FL, USA: CRC Press, Oct. 2018, pp. 179–204.

[54] Z. Průša and P. L. Søndergaard, "Real-time audio visualization with reassigned non-uniform filter banks," in *Proc. Int. Conf. Digit. Audio Effects (DAFx)*, Sep. 2016, pp. 3–8.

[55] C. K. Chui, Y.-T. Lin, and H.-T. Wu, "Real-time dynamics acquisition from irregular samples—With application to anesthesia evaluation," *Anal. Appl.*, vol. 14, no. 4, pp. 537–590, Jul. 2016.

[56] P. L. Søndergaard, "Efficient algorithms for the discrete Gabor transform with a long FIR window," *J. Fourier Anal. Appl.*, vol. 18, no. 3, pp. 456–470, Jun. 2012.

[57] P. Bloomfield, *Fourier Analysis of Time Series: An Introduction*, 2nd ed. New York, NY, USA: Wiley, 2000.

[58] G. H. Golub, "Some modified matrix eigenvalue problems," *SIAM Rev.*, vol. 15, no. 2, pp. 318–334, Apr. 1973.

[59] J. R. Weaver, "Centrosymmetric (cross-symmetric) matrices, their basic properties, eigenvalues, and eigenvectors," *Amer. Math. Monthly*, vol. 92, no. 10, pp. 711–717, Dec. 1985.

[60] J. McClellan and T. Parks, "A unified approach to the design of optimum FIR linear-phase digital filters," *IEEE Trans. Circuit Theory*, vol. CT-20, no. 6, pp. 697–701, Nov. 1973.

[61] D. M. Gruenbacher and D. R. Hummels, "A simple algorithm for generating discrete prolate spheroidal sequences," *IEEE Trans. Signal Process.*, vol. 42, no. 11, pp. 3276–3278, 1994.
[62] T. Verma, S. Bilbao, and T. Meng, "The digital prolate spheroidal window," in *Proc. IEEE Int. Conf. Acoust., Speech, Signal Process. (ICASSP)*, vol. 3, May 1996, pp. 1351–1354.
[63] X. Lai, "Constrained Chebyshev design of FIR filters," *IEEE Trans. Circuits Syst. II, Exp. Briefs*, vol. 51, no. 3, pp. 143–146, Mar. 2004.
[64] J. H. McClellan, T. W. Parks, and L. Rabiner, "A computer program for designing optimum FIR linear phase digital filters," *IEEE Trans. Audio Electroacoust.*, vol. AU-21, no. 6, pp. 506–526, Dec. 1973.
[65] X. Lai, "Chebyshev design of FIR filters with frequency inequality constraints," *Circuits, Syst., Signal Process.*, vol. 22, no. 3, pp. 181–193, Mar. 2003.
[66] M. J. D. Powell, *Approximation Theory and Methods*. New York, NY, USA: Cambridge Univ. Press, 1981.
[67] R. G. Baraniuk, P. Flandrin, A. J. E. M. Janssen, and O. J. J. Michel, "Measuring time-frequency information content using the Rényi entropies," *IEEE Trans. Inf. Theory*, vol. 47, no. 4, pp. 1391–1409, May 2001.
[68] S. Meignen, D.-H. Pham, and S. McLaughlin, "On demodulation, ridge detection, and synchrosqueezing for multicomponent signals," *IEEE Trans. Signal Process.*, vol. 65, no. 8, pp. 2093–2103, Apr. 2017.
[69] S. Meignen, M. Colominas, and D.-H. Pham, "On the use of Rényi entropy for optimal window size computation in the short-time Fourier transform," in *Proc. IEEE Int. Conf. Acoust., Speech Signal Process. (ICASSP)*, May 2020, pp. 5830–5834.
[70] O. Pele and M. Werman, "Fast and robust earth mover's distances," in *Proc. IEEE Int. Conf. Comput. Vis. (ICCV)*, Sep. 2009, pp. 460–467.
[71] I. Daubechies, Y. Wang, and H.-T. Wu, "ConceFT: Concentration of frequency and time via a multitapered synchrosqueezed transform," *Phil. Trans. Roy. Soc. A, Math., Phys. Eng. Sci.*, vol. 374, no. 2065, Apr. 2016, Art. no. 20150193.

TSUBASA KUSANO (Graduate Student Member, IEEE) received the B.E. and M.E. degrees from Waseda University, Tokyo, Japan, in 2017 and 2018, respectively, where he is currently pursuing the Ph.D. degree with the Department of Intermedia Art and Science. His research interests include signal processing based on functional data analysis and time-frequency analysis.

KOHEI YATABE (Member, IEEE) received the B.E., M.E., and Ph.D. degrees from Waseda University, in 2012, 2014, and 2017, respectively. He is currently an Assistant Professor with the Department of Intermedia Art and Science, Waseda University.

YASUHIRO OIKAWA (Member, IEEE) received the B.E., M.E., and Ph.D. degrees in electrical engineering from Waseda University, in 1995, 1997, and 2001, respectively. He is currently a Professor with the Department of Intermedia Art and Science, Waseda University. His research interests include communication acoustics and digital signal processing of acoustic signals. He is a member of ASJ, ASA, IEICE, IPSJ, VRSJ, and AIJ.